The Atlastin ER-shaping proteins facilitate Zika virus replication

Blandine Monel, Maaran Michael Rajah, Mohamed-Lamine Hafirassou, Samy Sid-Ahmed, Julien Burlaud-Gaillard, Peng-Peng Zhu, Quentin Nevers, Julian Buchrieser, Françoise Porrot, Cécile Meunier, et al.

Journal of Virology®

VIRUS-CELL INTERACTIONS

Atlastin Endoplasmic Reticulum-Shaping Proteins Facilitate Zika Virus Replication

Blandine Monel,[a] Maaran Michael Rajah,[a,b] Mohamed Lamine Hafirassou,[c] Samy Sid Ahmed,[a] Julien Burlaud-Gaillard,[d] Peng-Peng Zhu,[e] Quentin Nevers,[a] Julian Buchrieser,[a] Françoise Porrot,[a] Cécile Meunier,[a] Sonia Amraoui,[a] Maxime Chazal,[f] Audrey Salles,[g] Nolwenn Jouvenet,[f] Philippe Roingeard,[d] Craig Blackstone,[e] Ali Amara,[c] Olivier Schwartz[a]

[a]Institut Pasteur, Virus and Immunity Unit, CNRS-UMR3569, Paris, France
[b]Ecole Doctorale Bio Sorbonne Paris Cité (BioSPC)–Université Paris Diderot, Paris, France
[c]Equipe Biologie Cellulaire des Infections Virales, INSERM U944 CNRS 7212, Centre de Recherche Saint-Louis, Paris, France
[d]INSERM U1259–Plateforme IBiSA de Microscopie Electronique, Université et CHU de Tours, Tours, France
[e]Cell Biology Section, Neurogenetics Branch, National Institutes of Health, Bethesda, Maryland, USA
[f]Institut Pasteur, Viral Genomics and Vaccination Unit, Paris, France
[g]Institut Pasteur, UtechS Photonic BioImaging PBI (Imagopole), Centre de Recherche et de Resources Technologiques C2RT, Paris, France

ABSTRACT The endoplasmic reticulum (ER) is the site for Zika virus (ZIKV) replication and is central to the cytopathic effects observed in infected cells. ZIKV induces the formation of ER-derived large cytoplasmic vacuoles followed by "implosive" cell death. Little is known about the nature of the ER factors that regulate flavivirus replication. Atlastins (ATL1, -2, and -3) are dynamin-related GTPases that control the structure and the dynamics of the ER membrane. We show here that ZIKV replication is significantly decreased in the absence of ATL proteins. The appearance of infected cells is delayed, the levels of intracellular viral proteins and released virus are reduced, and the cytopathic effects are strongly impaired. We further show that ATL3 is recruited to viral replication sites and interacts with the nonstructural viral proteins NS2A and NS2B3. Thus, proteins that shape and maintain the ER tubular network ensure efficient ZIKV replication.

IMPORTANCE Zika virus (ZIKV) is an emerging virus associated with Guillain-Barré syndrome, and fetal microcephaly as well as other neurological complications. There is no vaccine or specific antiviral treatment against ZIKV. We found that endoplasmic reticulum (ER)-shaping atlastin proteins (ATL1, -2, and -3), which induce ER membrane fusion, facilitate ZIKV replication. We show that ATL3 is recruited to the viral replication site and colocalize with the viral proteins NS2A and NS2B3. The results provide insights into host factors used by ZIKV to enhance its replication.

KEYWORDS atlastin, Zika, endoplasmic reticulum

Flaviviruses are transmitted to vertebrate hosts by mosquitoes or ticks. Dengue virus (DENV), Yellow fever virus (YFV), West Nile virus (WNV), and Zika virus (ZIKV) are highly pathogenic to humans and constitute major international health problems. The recent ZIKV epidemics, associated with neurological disorders such as Guillain-Barré syndrome and microcephaly, provoked a public health emergency in 2016 (1, 2). An intensive research effort led to important progress regarding ZIKV epidemiology, diagnosis, and potential therapeutic and prophylactic strategies (3–5). The mechanisms involved in ZIKV replication, host responses, and pathogenesis have also been extensively studied (6, 7). However, the role of cellular proteins, in particular those present in the endoplasmic reticulum (ER), where viral production occurs, remains only partly characterized.

The ZIKV genome consists of a single-stranded positive-sense RNA encoding a

Citation Monel B, Rajah MM, Hafirassou ML, Sid Ahmed S, Burlaud-Gaillard J, Zhu P-P, Nevers Q, Buchrieser J, Porrot F, Meunier C, Amraoui S, Chazal M, Salles A, Jouvenet N, Roingeard P, Blackstone C, Amara A, Schwartz O. 2019. Atlastin endoplasmic reticulum-shaping proteins facilitate Zika virus replication. J Virol 93:e01047-19. https://doi.org/10.1128/JVI.01047-19.

Editor Mark T. Heise, University of North Carolina at Chapel Hill

Address correspondence to Blandine Monel, blandine.monel@pasteur.fr, or Olivier Schwartz, olivier.schwartz@pasteur.fr.

B.M. and M.M.R. contributed equally to this article.

Received 21 June 2019
Accepted 8 September 2019
Accepted manuscript posted online 18 September 2019
Published 13 November 2019

polyprotein precursor that gives rise to seven nonstructural (NS) and three structural proteins (capsid C, premembrane prM, and envelope E). Cellular receptors for the virus include AXL and Tim-1 (8, 9). After endocytosis, pH-dependent fusion of viral and endosomal membranes, uncoating, and release of the viral material into the cytoplasm, the subsequent steps of the viral life cycle, including RNA replication, synthesis of viral proteins, and particle assembly, take place in the ER (10–15). The viral genome serves as mRNA for protein synthesis (16, 17). The viral polyprotein is processed by cellular and viral (NS3/NS2B, also termed NS2B3) proteases. NS proteins form a replication complex (RC) with cellular factors that induces membrane rearrangements and formation of novel organelles (14, 18, 19). NS2A and NS4A/B proteins contain helices that reside in the plane of the ER-luminal membrane leaflets, thereby increasing their surface. The membrane curvature is further induced by oligomerization of NS4A, which interacts with NS4B and NS1. There, the viral positive-strand RNA is copied into a negative-strand intermediate that serves as a template for RNA replication performed by NS5 polymerase and NS3 helicase (14, 20).

Remodeling of the ER and accumulation of viral proteins trigger a stress pathway and activate the unfolded protein response (UPR) (21–23). Uncontrolled UPR response leads to cell death and instigate inflammation. We recently showed that ZIKV induces massive ER-derived vacuolization and UPR, followed by paraptosis, a nonapoptotic form of cell death (23). Therefore, in addition to serving as the site for virus replication and production, the ER is central to the death of infected cells.

The ER is a complex architecture of membranes comprising the nuclear envelope, peripheral sheets, and an interconnected network of tubules. The structure and dynamic nature of the ER allow it to be involved in many processes, including protein production and degradation, cell signaling, and the synthesis and distribution of lipids. Several proteins that shape the ER have been identified. Proteins of the reticulon (RTN) and receptor expression enhancing protein (REEP) families generate curves in membranes and act to maintain the tubules (24–26). Atlastin proteins (ATLs) mediate the tethering and fusion of tubules to one other to form three-way junctions (27, 28), which are stabilized by the Lunapark protein (26). ATLs are large dynamin-related GTPases that dimerize in *cis* and *trans* to allow fusion of adjacent ER membranes. Humans have three ATLs (ATL1, ATL2, and ATL3), with redundant activities and various levels of expression in different cell types (29). Several other proteins help the ER to maintain contact with the plasma membrane, other compartments, and the cytoskeleton (25). Mutations in ATL1 and ATL3 or other ER-shaping proteins are associated with neurological diseases, such as hereditary sensory neuropathy and spastic paraplegia, and are characterized by axon and dendrite growth deficits (30–36).

Reticulon 3.1A (RTN3.1A) is used by flaviviruses to facilitate ER membrane remodeling (37), but the role of other ER-shaping proteins is uncharacterized. Here, we report that ATL proteins enhance ZIKV replication and cytopathic effects. We further characterize the underlying viral and cellular mechanisms and report that ATL3 is recruited to viral replication sites and interacts with NS2A and NS2B3.

RESULTS

Silencing of the ATL proteins impairs ZIKV replication and vacuole formation. We first sought to determine whether ATLs impact ZIKV spread. HeLa cells express ATL2 and ATL3 and background levels of ATL1 (29). We silenced ATL1, -2, and -3 (ATL1/2/3) by using small interfering RNA (siRNA) in these cells. As a positive control, we silenced dolichyl-diphosphooligosaccharide protein glycosyltransferase (DDOST), an ER enzyme required for ZIKV replication (38–41). Silencing reduced by 80 to 90% the levels of ATL1/2/3 or DDOST mRNA, respectively, as measured by quantitative reverse transcription-PCR (RT-qPCR), without affecting cell viability (Fig. 1A and B). HeLa cells were then challenged with an African isolate of ZIKV (HD78788, referred to as HD78) at different multiplicities of infection (MOIs). Viral replication was followed over time by flow cytometry, by measuring the frequency of cells harboring the viral envelope (E) protein, using the pan-flavivirus anti-E antibody 4G2 (Fig. 1C). Silencing of ATL significantly

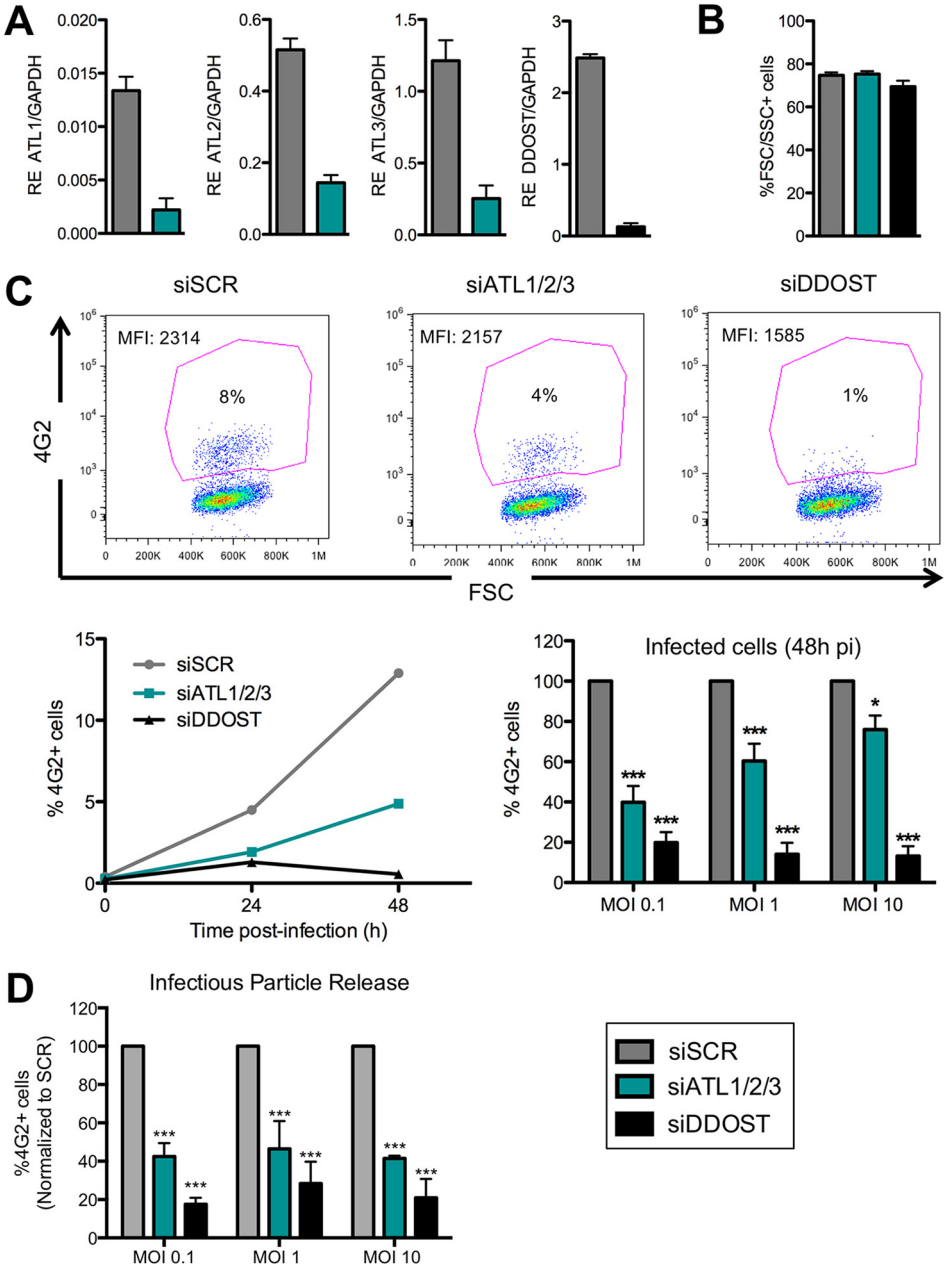

FIG 1 Silencing of ATL impairs ZIKV replication. (A) HeLa cells were transfected with siRNAs targeting a control scrambled RNA (siSCR), dolichyl-diphosphooligosaccharide–protein glycosyltransferase RNA (siDDOST), or targeting ATL1, ATL2, and ATL3 (siATL1/2/3). The efficiency of the silencing was checked by RT-qPCR at 3 days posttransfection. The relative expression of each RNA compared to GAPDH is shown. (B) Cell viability was assessed by flow cytometry after 4 days of siRNA treatment using forward- and side-scatter parameters. (C) Cells were infected with ZIKV HD78 (at the indicated MOI), and the percent E-positive cells was determined by flow cytometry at 48 h p.i. using 4G2 antibody. (Upper panel) Representative experiment (MOI of 1 at 48 h p.i.) showing fluorescence-activated cell sorting (FACS) dot plots. (Left panel) Representative experiment showing kinetics (MOI of 1). (Right panel) Means ± the standard errors of the mean (SEM) of five independent experiments at 48 h p.i. (D) Supernatants from infected cells (at 24 h p.i.) were used to infect fresh HeLa cells. The percent E-positive cells was determined at 24 h p.i. The means ± the SEM of three independent experiments are shown. Statistical significance was determined by using analysis of variance (ANOVA) and Bonferroni posttests. ***, $P < 0.001$; **, $P < 0.01$; *, $P < 0.05$.

decreased viral replication. The effect of ATL silencing was more marked at a low MOI. As expected, ZIKV replication was abrogated in the absence of DDOST. We next assessed the release of infectious virus in the medium. To this aim, supernatants were harvested at 24 h and exposed to fresh cells. The release of infectious

particles was significantly decreased in cells where ATL or DDOST had been silenced (Fig. 1D).

We previously described the appearance of large ER-derived cytoplasmic vacuoles in ZIKV infected cells (23). In ATL-silenced ZIKV-infected HeLa cells, the formation of these vacuoles was strongly decreased at 24 h, as assessed by light microscopy and visual scoring (Fig. 2A and B). The fraction of cells displaying vacuoles remained low, even at a high viral inoculum (MOI of 10) and at a later time point (48 h postinfection [p.i.]), when about 60% of the cells were $4G2^+$. To provide ultrastructural detail, we performed transmission electron microscopy of ZIKV-infected cells at 24 h p.i. (MOI of 10) (Fig. 2C). As expected, large intracellular vacuoles were observed in control infected cells. These vacuoles were much smaller and rarer in the absence of ATL (Fig. 2). In infected cells treated with the control RNAi, we observed membrane alterations and electron-dense structures with enlarged ERs, convoluted membranes, and spherule-like structures (Fig. 3). Virions were observed in these rearranged structures as single or clustered particles within membrane invaginations (Fig. 3). A similar alteration of the ER morphology and the presence of virus particles were observed in ATL-silenced cells. It was difficult to precisely quantify the number of vesicle pockets containing virions with this technique. However, at the high MOI required for transmission electron microscopy experiments, we observed a trend to a decreased number of pockets in the absence of ATL (Fig. 3).

We next examined the role of ATL1/2/3 in primary human adult dermal fibroblasts (HDFa), which represent natural target cells for the virus upon mosquito bite. Silencing of ATL1/2/3 by siRNA resulted in decreased production of viral proteins (Fig. 4A to C). The large intracellular vacuoles were no longer visible in the absence of ATL (Fig. 4D).

ZIKV replication and cytopathic effects in ATL KO cells. To further characterize the role of ATL, we generated an ATL 2/3 double-knockout (dKO) HeLa cell clone, termed 21/1 dKO (and referred to here as dKO) by CRISPR-mediated gene editing (42). We did not target ATL1, which is expressed at background levels in HeLa cells. In dKO cells, DNA sequencing revealed mutations prematurely truncating ATL proteins (42; also, data not shown). Western Blot with an anti-ATL3 antibody confirmed a strong decrease of protein levels in dKO cells, compared to parental (WT) cells (Fig. 5A). We could not assess ATL2 levels, due to the lack of commercially available antibodies. As controls, we stably reexpressed a wild-type (WT) or a GTPase-deficient (ATL3 KA) mutant in dKO cells. We also introduced a wild-type myc-tagged protein (ATL3 myc) to facilitate imaging studies. These proteins were readily detected by Western blotting in reconstituted cells (Fig. 5A). As previously described in another cell line (3T3-derived cells) (42), the shape of the ER was modified in dKO cells (Fig. 5B). Staining of the cells with a red fluorescent ER tracker and analysis by super-resolution microscopy demonstrated a disrupted peripheral ER tubular network. These morphology changes were rescued by WT ATL3 or ATL3-myc, whereas cells expressing the GTPase-defective ATL3KA mutant retained an abnormal ER (Fig. 5B).

We then assessed ZIKV replication in these cells. Viral spread was decreased by more than 2-fold in dKO cells compared to WT cells (Fig. 6A), confirming the results obtained with siRNAs. Viral replication was rescued in dKO reexpressing WT ATL3 and not the KA mutant (Fig. 6A). We also observed a marked decrease of vacuole formation in dKO-infected cells (Fig. 6B). Again, reexpression of WT, but not that of ATL3 KA mutant, restored a rapid appearance of vacuoles. At a later time point (72 h p.i.), the fraction of dying cells was augmented in the presence of functional ATL3 proteins (Fig. 6C). As observed with siRNAs, the release of infectious particles was also significantly decreased in dKO cells and rescued with ATL3, as assessed by a flow-cytometry based assay. These results were also supported by a traditional plaque assay (data not shown). In addition to the African ZIKV strain HD78, replication of three Asian-lineage strain (FG16, PF13, and NC14) ZIKV isolates was also impaired in the absence of ATL (Fig. 6D).

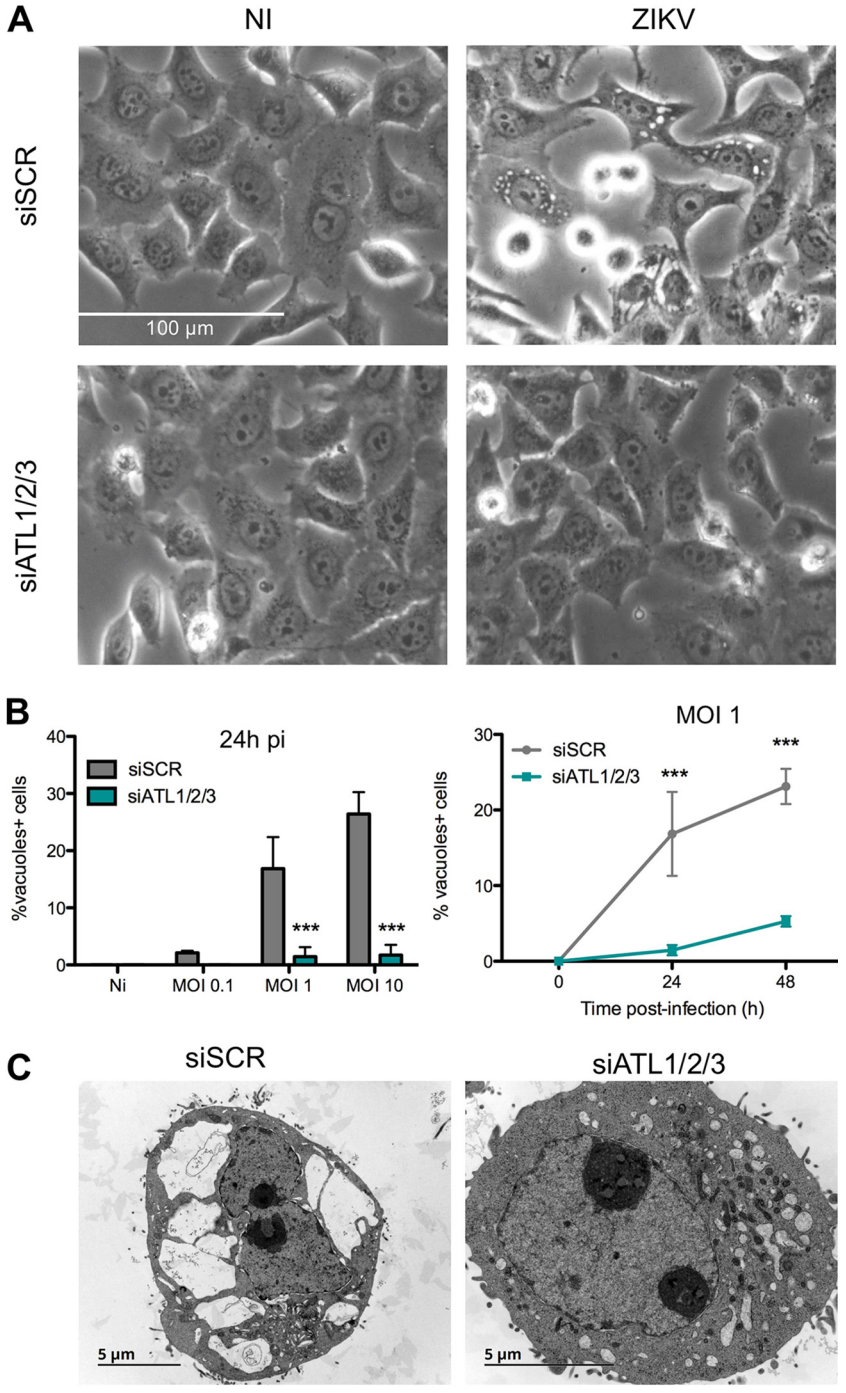

FIG 2 Silencing of ATL impairs ZIKV-induced vacuoles. (A) HeLa siSCR or siATL1/2/3 cells infected or not with ZIKV (MOI of 10) were observed by light microscopy at 24 h p.i. to visualize virus-induced vacuoles. (B) Cells infected with ZIKV were observed by light microscopy at 24 h p.i., and the percentage of vacuole-positive cells was calculated. (C) HeLa siSCR or siATL1/2/3 cells infected or not with ZIKV (MOI of 10) were observed by transmission electron microscopy at 24 h p.i. to visualize virus-induced vacuoles. (Left) Percent vacuoles and cells quantified at 24 h p.i. at the indicated MOI. (Right) Percent vacuoles and cells at the indicated times (MOI of 1). The means ± the SEM of three independent experiments are shown. Statistical significance was determined by using ANOVA and Bonferroni posttests. ***, $P < 0.001$.

To rule out a clone-dependent effect on ZIKV replication, we used another HeLa dKO clone. In the absence of infection, the viability and growth kinetics of the two dKO clones were similar to the parental HeLa cells. ZIKV replication was impaired in both clones (not shown).

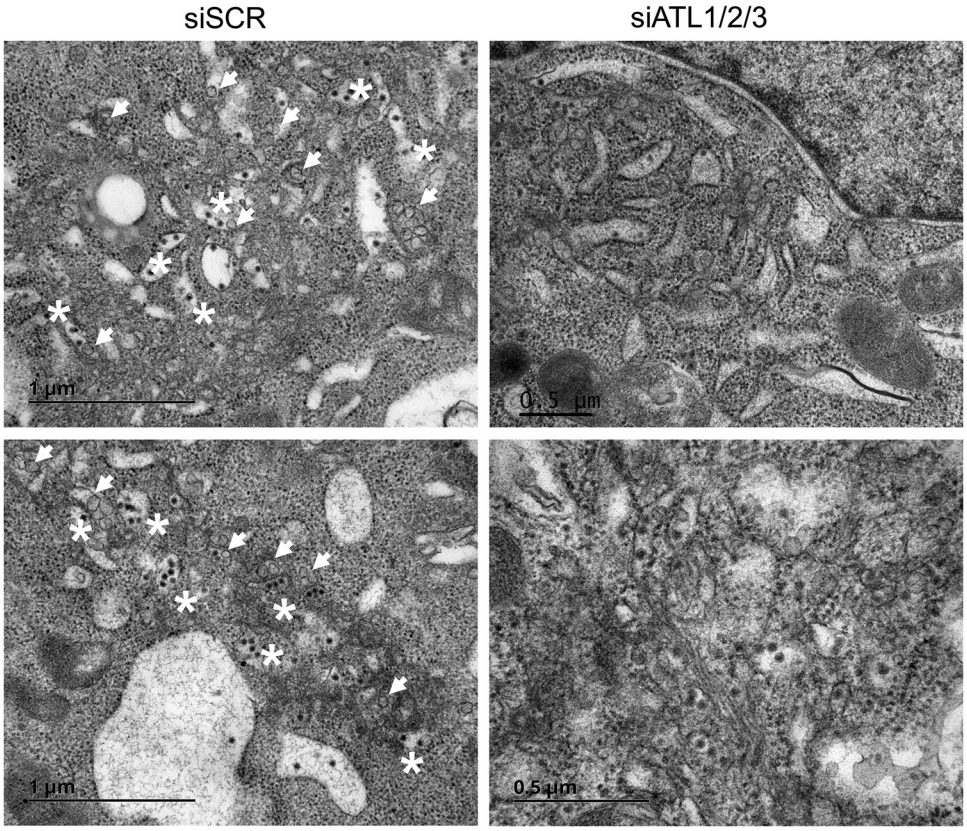

FIG 3 Ultrastructural analysis of ZIKV-infected HeLa cells. HeLa siSCR or siATL1/2/3 cells infected with ZIKV (MOI of 10) were observed by electron microscopy at 24 h p.i. Two representative pictures are shown for each condition. White arrows, examples of ZIKV-induced spherules (vRNA replication); white asterisks, examples of viral particles.

Altogether, our results obtained in either silenced or knocked out cells indicate that ATL proteins facilitate the replication of ZIKV strains of different origins and enhance the formation of ER-derived vacuoles in infected cells.

ER modifications in ZIKV-infected WT and dKO cells. ZIKV infection induces a profound modification of the topography of ER that can be visualized by immunofluorescence or transmission electron microscopy. To study the impact of ATL on these changes, we generated WT or dKO cells stably expressing a fluorescent Sec61β-mEmmerald protein (Fig. 7). Sec61 is the main protein translocation complex of the ER membrane. As expected, in the absence of infection, in HeLa WT cells, Sec6β was mainly detected in a perinuclear region, associated with a dispersed staining throughout the cytoplasm. A similar global pattern was observed in dKO cells. Analysis by super-resolution confirmed the presence of an abnormal tubular ER (not shown).

We visualized cells using time-lapse fluorescence microscopy after incubation with virus, with images acquired every 5 min for up to 24 h. Representative examples are shown in Fig. 7A (see also Videos S1 and S2 in the supplemental material). In both WT and dKO cells, ZIKV modified the aspect of the ER, with a condensation and intensification the Sec61β signal that was visible at 12 to 16 h p.i. In WT cells, this contraction of the ER was followed by formation of cytoplasmic vacuoles and cell death (Fig. 7A; see Videos S1 and S2). The vacuoles were surrounded by Sec61β, supporting our finding that they originate from the ER (23). In dKO cells, the changes in ER topology were much less associated with vacuolization (Fig. 7), confirming our results obtained by optic and electron microscopy (Fig. 2). We then examined viral production sites and ATL localization by confocal microscopy. As expected, in both WT and dKO cells, the viral protein E accumulated in the ER, in a region enriched for Sec61β (Fig. 7B). In noninfected cells, ATL3, visualized with an anti-myc antibody, appeared as a dispersed signal

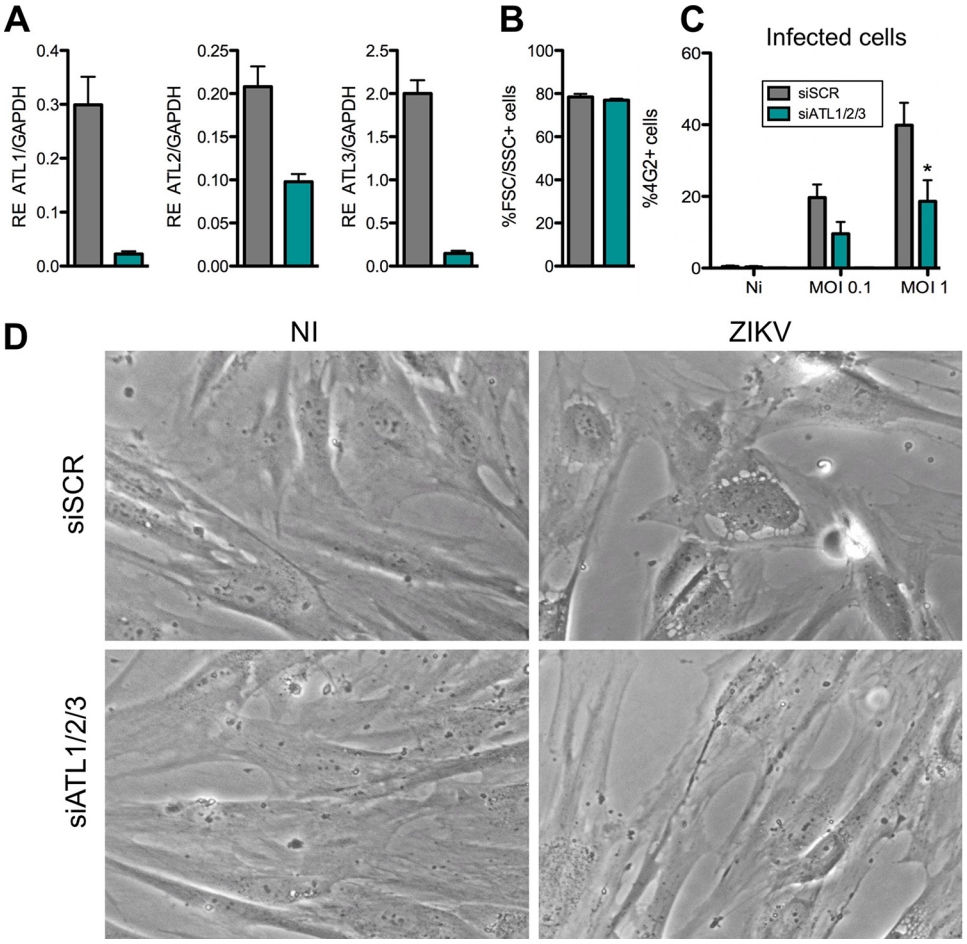

FIG 4 Silencing of ATL impairs ZIKV replication in primary adult human dermal fibroblast (HDFa) cells. (A) HDFa cells were transfected with siRNAs targeting a control scrambled RNA (siSCR) or targeting ATL1, ATL2, and ATL3 (siATL1/2/3). The efficiency of the silencing was checked by RT-qPCR at 3 days posttransfection. The relative expression of each RNA compared to GAPDH is shown. (B) Cell viability was assessed by flow cytometry after 4 days of siRNA treatment using forward- and side-scatter parameters. (C) Cells were infected with ZIKV HD78 (at the indicated MOI), and the percent E-positive cells was determined by flow cytometry at 48 h p.i. using 4G2 antibody. (Left) Representative experiment (MOI of 1). (Right) Means ± the SEM of three independent experiments at 48 h p.i. The statistical significance was determined by using ANOVA and Bonferroni posttests. *, $P < 0.05$. (D) Cells infected or not with ZIKV (MOI of 1) were observed by light microscopy at 24 h p.i. to visualize virus-induced vacuoles.

throughout the cytoplasm, with dots that likely correspond to three-way ER junctions (26) (Fig. 8). ZIKV induced a profound modification of ATL3 repartition, corresponding to ER morphological changes (Fig. 8).

Therefore, ATL3 is present at viral replication or viral production sites. In infected cells, ATLs are not required for global ER rearrangements triggered by the virus but enhance the formation of vacuoles and cytopathic effects.

ATLs enhance viral production after ZIKV entry and interact with NS proteins. We next studied how ATL positively impacts ZIKV spread. We first measured viral binding and entry in HeLa WT and dKO cells. The cells were exposed to ZIKV for 1 h at 4°C at two MOIs. The viral input was then removed, and half of the cells were harvested to quantify bound particles. The other half was kept at 37°C for two additional hours to allow endocytosis and fusion, and extracellular bound particles were removed with a trypsin treatment. Trypsin eliminated >90% of bound viral RNA (not shown). Viral RNA was quantified by RT-qPCR (Fig. 9A and B). The signal was proportional to the MOI, indicating that nonsaturating conditions were used. We did not observe any difference in viral binding and entry between the two cell types. To further study the impact of

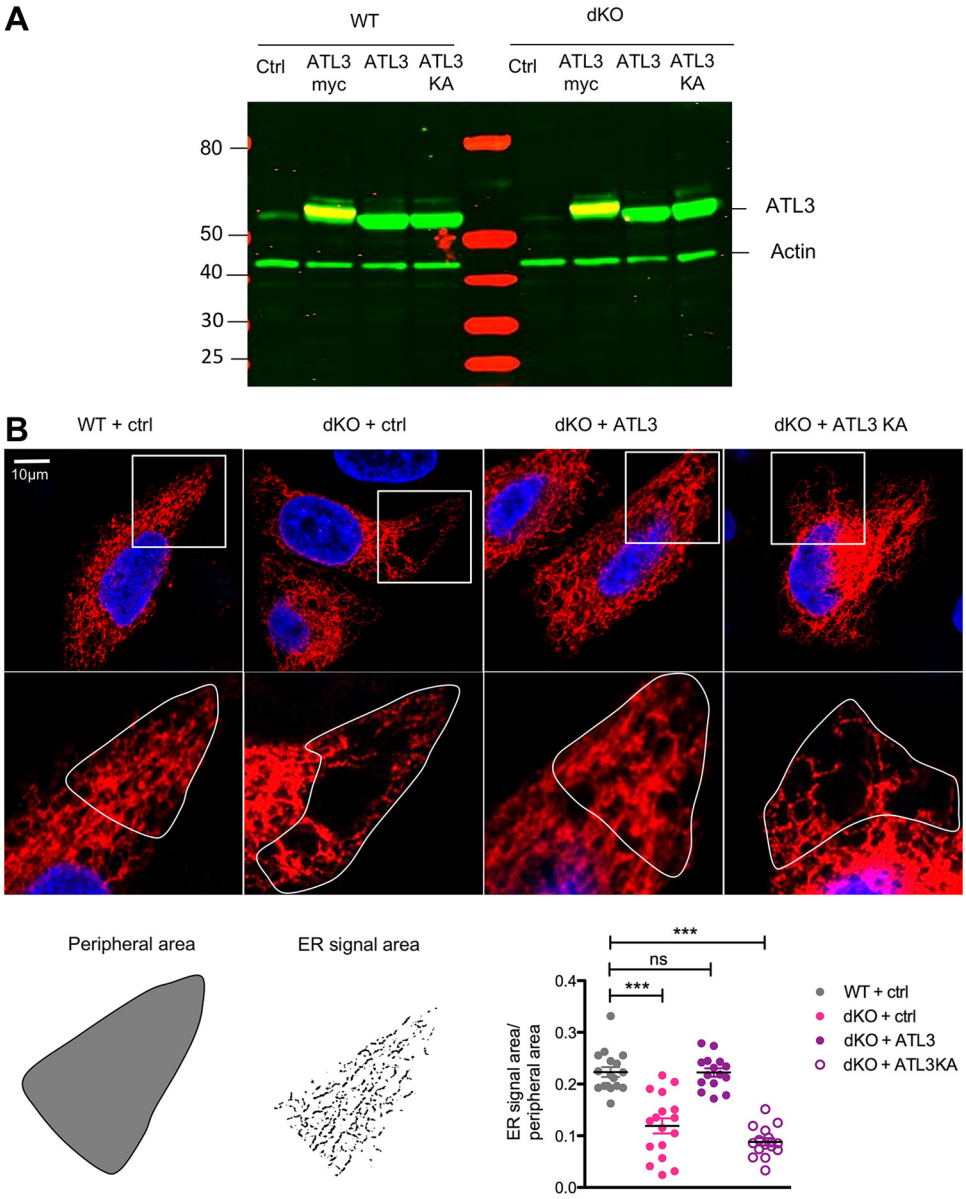

FIG 5 Characterization of ATL KO HeLa cells. (A) HeLa cells were knocked out for ATL2 and ATL3 genes (dKO) using CRISPR. HeLa WT or dKO cells were then transduced to express exogenous ATL3-myc, ATL3 WT, or ATL3 mutated in the GTPase activity domain (ATL3KA). ATL3 expression was assessed by Western blotting. Actin was used as a loading control. (B) HeLa WT or dKO cells transduced with control (ctrl), ATL3 WT, or ATL3KA vectors and expressing an ER-tracker dsRed2 were examined by confocal microscopy to observe the structure of the peripheral ER tubular network. Three-way junctions were quantified as previously described (42). At least three cells per condition per experiment from three independent experiments were analyzed and plotted. Statistical significance was determined by using a one-way ANOVA test and a Dunnett posttest. ***, $P < 0.001$.

ATLs on viral RNA amplification, we transfected WT and dKO cells with RNA produced from a ZIKV infectious clone expressing a reporter luciferase (43). The ZIKV RNA triggered a luciferase signal that increased over time in WT cells and remained low in dKO cells (Fig. 9C). Similar results were obtained when cells were treated with NH_4Cl, an inhibitor of vesicular acidification that prevents secondary cycles of viral replication (Fig. 9C). Therefore, ATLs do not improve the early steps of the viral life cycle but facilitate viral RNA production and/or accumulation after viral entry.

We hypothesized that ATL may interact with NS proteins, as previously suggested in an interactome study (44). To test this hypothesis, we performed a coimmunoprecipitation of ATL3-myc and individual NS-HA proteins upon transfection in 293T cells. This

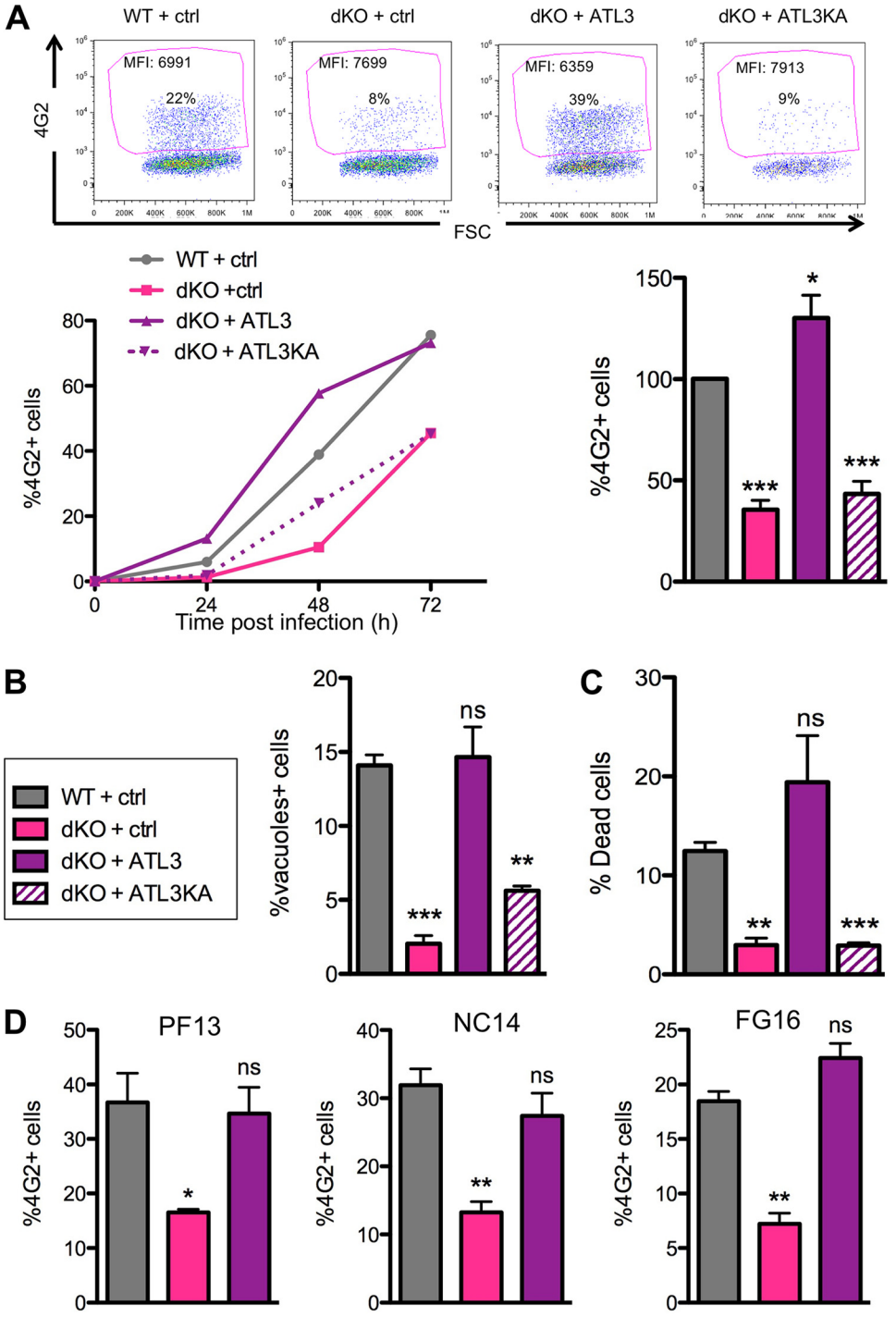

FIG 6 Knockout of ATL impairs ZIKV replication. (A) HeLa WT or dKO cells, transduced with control (ctrl), ATL3 WT, or ATL3KA vectors were infected with ZIKV (MOI of 0.1). The percentage of E^+ cells was monitored over time by flow cytometry using 4G2 antibody. (Upper panels) Representative FACS dot plots. (Lower left panel) A representative experiment. (Lower right panel) Means ± the SEM of five independent experiments at 48 h p.i. (B) Percent vacuoles and cells quantified at 24 h p.i. (MOI of 1). The means ± the SEM of three independent experiments are shown. (C) The percent dead cells were quantified at 72 h p.i. (MOI of 0.1) by Live/Dead staining and flow cytometry. The means ± the SEM of three independent experiments are shown. (D) HeLa WT or dKO cells transduced with control (ctrl) or ATL3 WT vectors were infected with ZIKV PF13, NC14, or ZIKV FG16 (MOI of 0.01), and the percent E^+ cells was determined by flow cytometry at 48 h p.i. The means ± the SEM of three independent experiments are shown. Statistical significance was determined by using a *t* test in comparison to the WT+Ctrl condition. ***, $P < 0.001$; **, $P < 0.01$; *, $P < 0.05$.

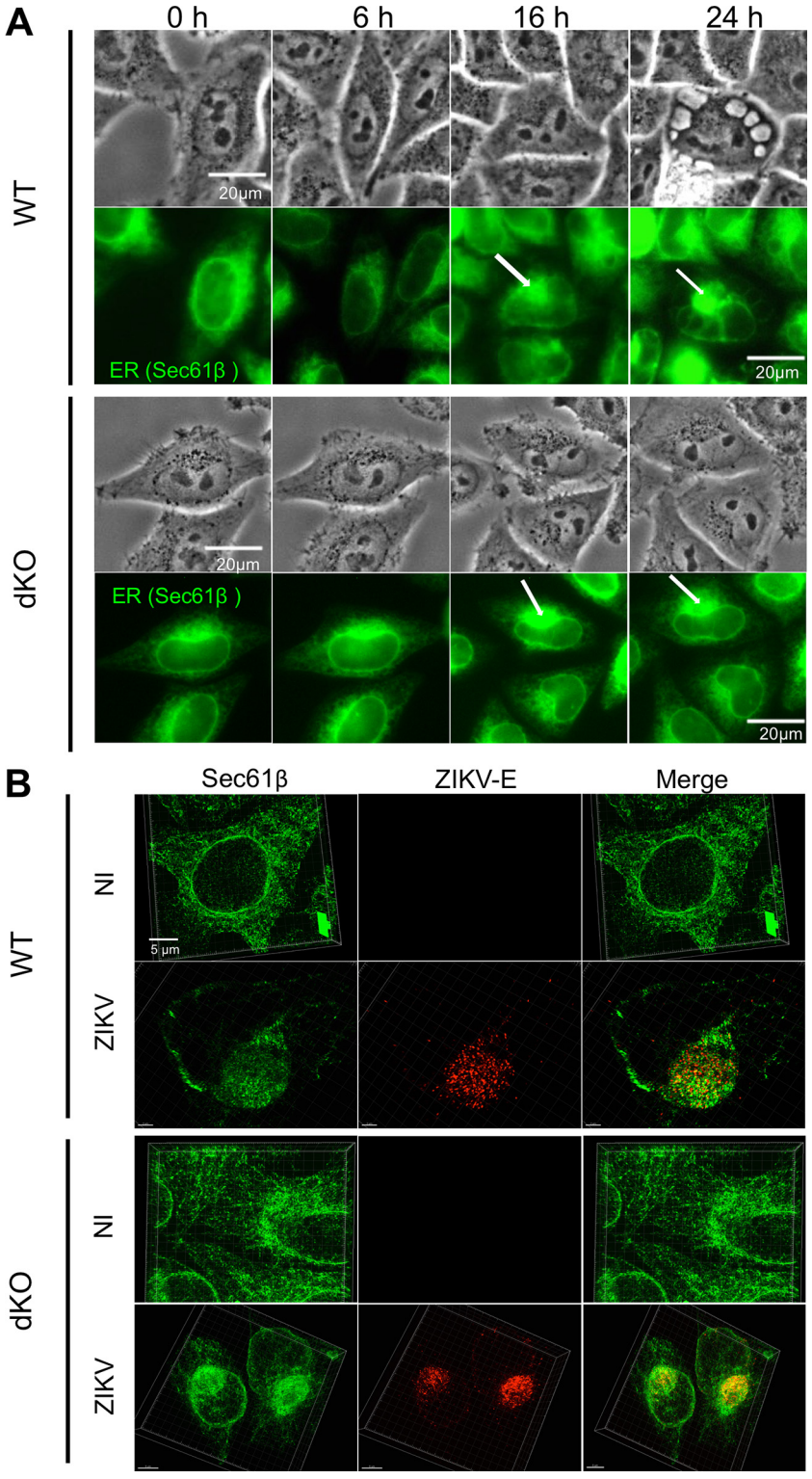

FIG 7 Impact of ATL on ZIKV-induced ER relocation. HeLa WT or dKO cells expressing a fluorescent Sec61β-mEmmerald ER protein (green) were infected with ZIKV (MOI of 1). (A) The ER structure was observed by time-lapse microscopy for 24 h. Still images extracted from Video S1 in the supplemental material are shown for transmitted light and Sec61β at the specified time points. White arrows indicate ZIKV-induced ER relocation. (B) HeLa WT or HeLa cells expressing Sec61β-mEmmerald (green) were infected or not for 24 h with ZIKV (MOI of 1). Cells were fixed and stained for the viral E protein (red) and observed by super-resolution imaging (SIM). A representative image is shown.

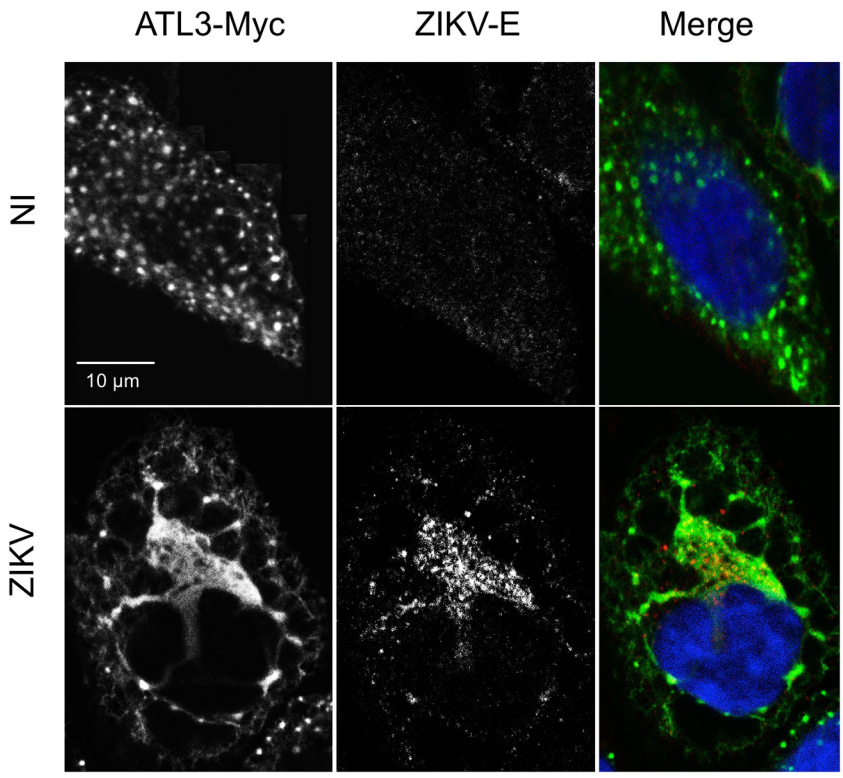

FIG 8 ATL3 is recruited to the viral replication site. HeLa cells expressing ATL3-myc were infected or not with ZIKV (MOI of 1) for 24 h. The cells were then fixed and stained for ATL3-myc (green) and viral E protein (white) and analyzed by confocal microscopy. A representative image is shown.

demonstrated an interaction between ATL3 and the NS2A and NS2B3 proteins, whereas the other NS proteins either did not associate or only poorly associated with ATL3 (Fig. 10A). Hemagglutinin (HA)-tagged NS2B3 and NS1 proteins were then transiently transfected in HeLa cells stably expressing ATL3-myc, and we examined the intracellular localization of the proteins by immunofluorescence. NS1 and NS2B3 displayed a punctuate staining which resembled that of ATL (Fig. 10B). Deconvolution of the images demonstrated a strong colocalization of ALT3 with NS2B3, and, to a much lower extent, with NS1 (Fig. 10B). To analyze NS3 and ATL3 localization in the context of viral infection, we infected HeLa dKO cells stably expressing ATL3-myc with ZIKV (MOI of 1 for 24 h) and stained the cells for NS3 and ATL3. We observed a strong colocalization between the two proteins (Fig. 11).

Altogether, these results indicate that ATL facilitates ZIKV production at the level of viral RNA and protein synthesis. ATL colocalizes and interacts with different NS proteins, mostly NS2A and NS2B3.

DISCUSSION

Flaviviruses such as ZIKV replicate their genomes in remodeled ER membranes (13, 18, 20). These viral factories allow the spatiotemporal control of the viral life cycle, ensures RNA amplification and production of viral proteins, and protects the viral RNA from the cytoplasmic environment and detection by sensors (13, 14). The ER is also central to ZIKV-induced cytopathic effect, which includes massive cellular vacuolization, triggering of an UPR response, and paraptosis-like cell death (21–23).

Genome-scale CRISPR and siRNA screens and proteomic analysis of cellular proteins associated with ZIKV or DENV proteins identified numerous host factors required for viral replication (38–41, 44–46). A large part of these host dependency factors are localized in the ER. For instance, (i) the ER membrane protein complex (EMC), which promotes the maturation of polytopic membrane proteins, (ii) the ER-associated pro-

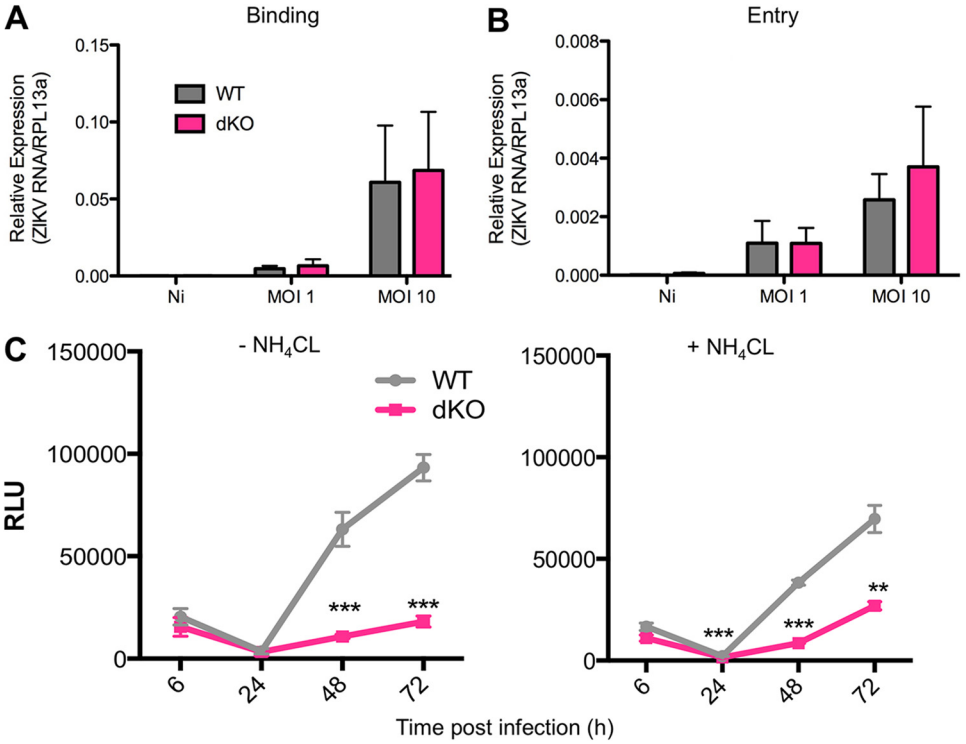

FIG 9 ATLs facilitate ZIKV replication after viral entry. (A) HeLa WT or dKO cells were exposed to ZIKV for 1 h at 4°C to allow viral binding. Viral input was washed out, and bound viral particles were quantified by RT-qPCR. The data are means ± the SEM of three independent experiments. (B) HeLa WT or dKO cells were exposed to ZIKV for 1 h at 4°C, washed out, and treated with trypsin to remove the bound viral particles. The cells were incubated at 37°C for 2 h to allow endocytosis and/or viral fusion. Intracellular viral RNA was quantified by RT-qPCR. Means ± the SEM of three independent experiments are shown. (C) HeLa WT or dKO cells were transfected with RNA from a ZIKV infectious clone expressing luciferase. The results are expressed in relative light units (RLU). The means ± the SEM of at least three independent experiments are shown. Statistical significance was determined using a *t* test, and each group was compared to the WT+ctrl condition. ***, $P < 0.001$; **, $P < 0.01$; *, $P < 0.05$.

tein degradation (ERAD), which targets misfolded proteins of the ER for ubiquitination and degradation by the proteasome, and (iii) the retrotranslocon Sec61, an oligosaccharyl transferase complex (OST) that glycosylates nascent proteins, are all required for ZIKV replication (38–41).

The role of ER-shaping proteins is less characterized. Reticulons (RTNs), atlastins (ATLs), receptor expression enhancing proteins (REEPs), and Lunapark regulate the structure and the dynamics of the ER compartment (25). These proteins were not identified in genomic screens of flavivirus infections. This suggests either that they are not important for viral replication or that the screening procedure may have missed this category of proteins for different reasons. One possible reason could be that their long-term deletion is deleterious to cell growth, independent of any infection. With other approaches than genome-wide screenings, it has been reported that RTN are required for the replication of enterovirus 71 and brome mosaic virus but negatively regulates hepatitis C virus (47–49). The RTN protein family is a large group of membrane-associated proteins involved in vesicle formation and membrane morphogenesis. RTNs control the formation of ER tubules and increase peripheral ER sheets (24, 50). Mutations in RTN2 are associated with hereditary spastic paraplegia disorders similarly to ATL1 (34). RTN3.1A is also required for the efficient replication of WNV, DENV-2, and ZIKV (37). In the absence of RTN3.1A, the number and size of ER membrane structures in flavivirus-infected cells are reduced (37). The impact of RTN3.1A on the viability of infected cells remains unknown.

We report that ATL enhance ZIKV spread by 2- to 3-fold. Reexpression of ATL3 in cells devoid of ATL restores viral replication. The three ATL display extensive homology,

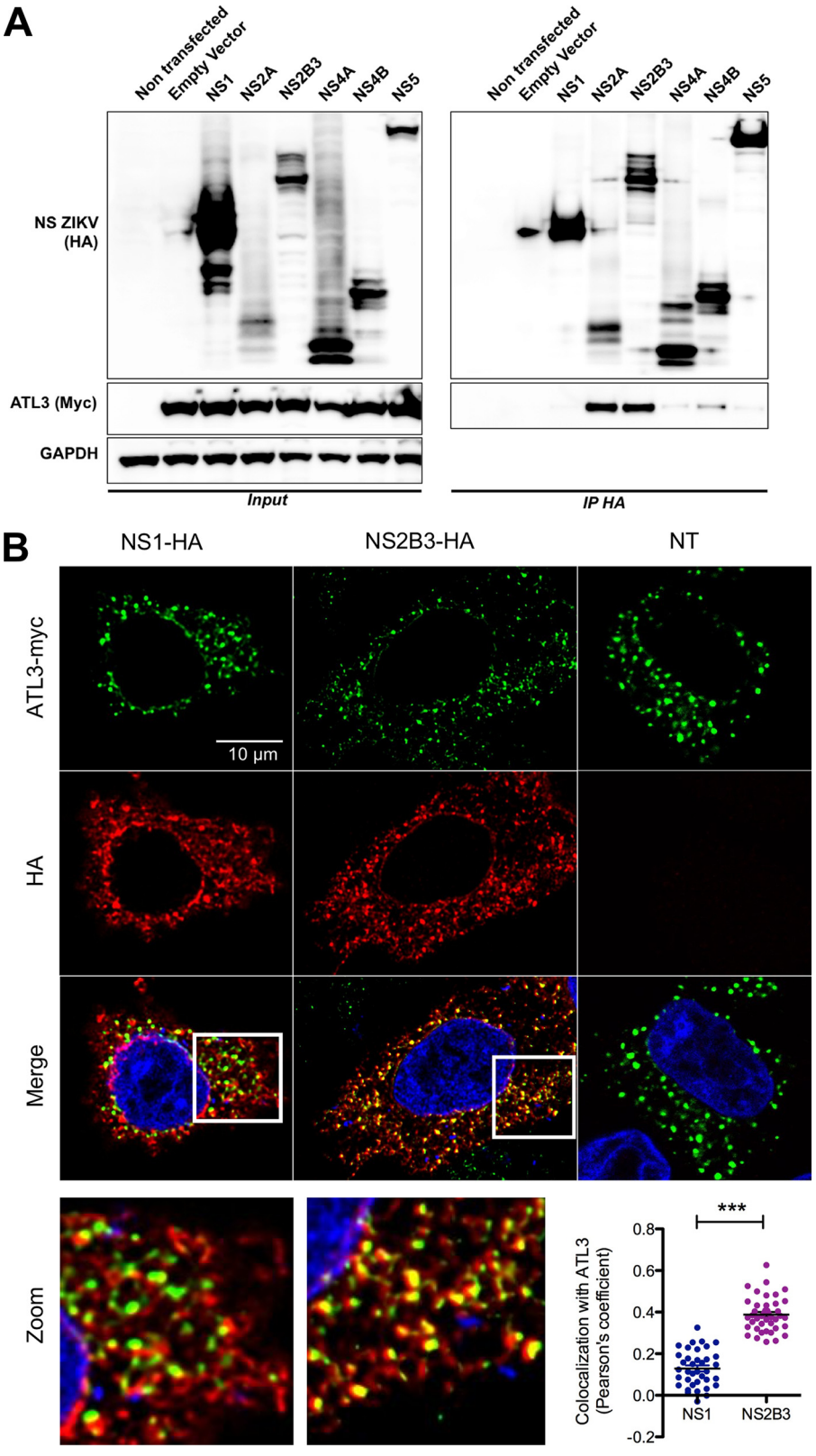

FIG 10 ATL3 colocalizes and interacts with ZIKV NS proteins. (A) HeLa cells expressing ATL3-myc were transfected with plasmids coding for individual NS-HA tagged proteins. NS proteins were eluted with an anti-HA antibody, and elution fractions were stained with an anti-myc antibody to detect coimmunoprecipitated ATL3. A representative blot from three independent experiments is shown. (B) HeLa cells expressing ATL3-myc were transfected with plasmids coding for HA-tagged NS1 or NS2B3 ZIKV proteins. The cells were fixed, stained for ATL3-myc (green) and NS-HA (red), and observed by confocal microscopy.

(Continued on next page)

with ATL1 being prominently expressed in neurons, and ATL2 and ATL3 more broadly in different cell types (51). It will be of interest to determineg whether the three ATL redundantly facilitate ZIKV replication. We further show that ATLs act after viral entry by increasing the levels of viral RNA and proteins. In the absence of ATL, the amounts of infectious virus released in the supernatants are strongly reduced. Our analysis of ZIKV-infected cells by confocal microscopy, video-microscopy, and electron microscopy indicates that intracellular structures associated with viral production are formed both in the presence and in the absence of ATL. We observed a similar condensation of the ER by immunofluorescence, with the appearance of an electron-dense region and vesicle pockets carrying viral particles. Distinct types of flavivirus-induced membrane alterations have been observed by electron tomography and other techniques (13, 18). The alterations include single-membrane invaginations of the ER, which may be associated with RNA synthesis, convoluted double membrane structures containing nonstructural proteins found in the vicinity of ER membranes, and invaginated vesicles (13, 18). Our electron microscopy results suggest that in the absence of ATLs, the number of such structures is decreased. Thus, since our results suggest a role for ATL at the replication step (Fig. 9), and given the endogenous role of ATL in ER membrane fusion/curvature, ZIKV likely overcomes the absence of ATL by replicating in viral factories that are much less efficiently formed than in presence of these proteins. It will be worth determining more precisely, by electron tomography and three-dimensional reconstruction, the characteristics and number of viral factories in cells that are either expressing or are deficient in ATL.

Membrane remodeling and accumulation of viral proteins in the ER trigger a stress pathway and activate the unfolded protein response (UPR) (5, 21, 23, 52). Knockout of ATL genes in mammalian cells alters ER sensitivity to UPR stress independently of any viral infection (42). We show here that in the absence of ATL, the appearance of large ER-derived vacuoles is strongly reduced, even at a high MOI. Moreover, the death of infected cells is attenuated without ATL. These observations strongly suggest that ATLs are key players in ZIKV-induced cytopathic effects, either directly or as a consequence of reduced viral replication. A decrease in the efficiency of cell death may also limit the release of infectious virus and further viral spread. Future work will help to determine whether the UPR response in ZIK-infected cells is impaired in the absence of ATL.

We report a recruitment of ATL3 to viral production sites and an interaction and colocalization of ATL3 with some NS proteins, mostly NS2A and NS2B3. We also show that the GTPase activity of ATL3 is required to enhance ZIKV replication and cytopathic effects. These observations raise interesting questions about the consequences of the interaction between NS proteins and ALT3. It will be worth determining whether this interaction modifies the enzymatic activity of ATL or stabilizes the formation or the function of the viral replication complex. RTN3.1 interacts with NS4A and protects NS4A from proteasomal degradation (37). It is tempting to speculate that the interaction of different NS proteins with various ER-shaping proteins may stabilize the docking of replication complexes and/or modulate the dynamics and structure of the ER to facilitate formation of viral factories. Alternatively, ER-shaping proteins could provide a dynamic environment for the creation of viral replication complexes, without requiring a direct interaction with NS proteins. Future work will help understanding the functional consequences of ATL-NS protein interaction. Furthermore, a recent study shows a role for ATL3 in ER export of cargo proteins into COPII vesicles (53). It would be of interest to determine whether ATL play also a role the transport or release of viral particles.

During flavivirus replication, a double-stranded intermediate RNA is produced and can be sensed in the cytoplasm by RIG-I-like receptors such as MD5 or RIG-I (54–57). It

FIG 10 Legend (Continued)
One field from a representative experiment is shown. Colocalization (Pearson's coefficient) was determined after deconvolution with Imaris software. At least 10 cells per condition (from three independent experiments) were plotted. Statistical significance was determined by using a *t* test ***, $P < 0.001$.

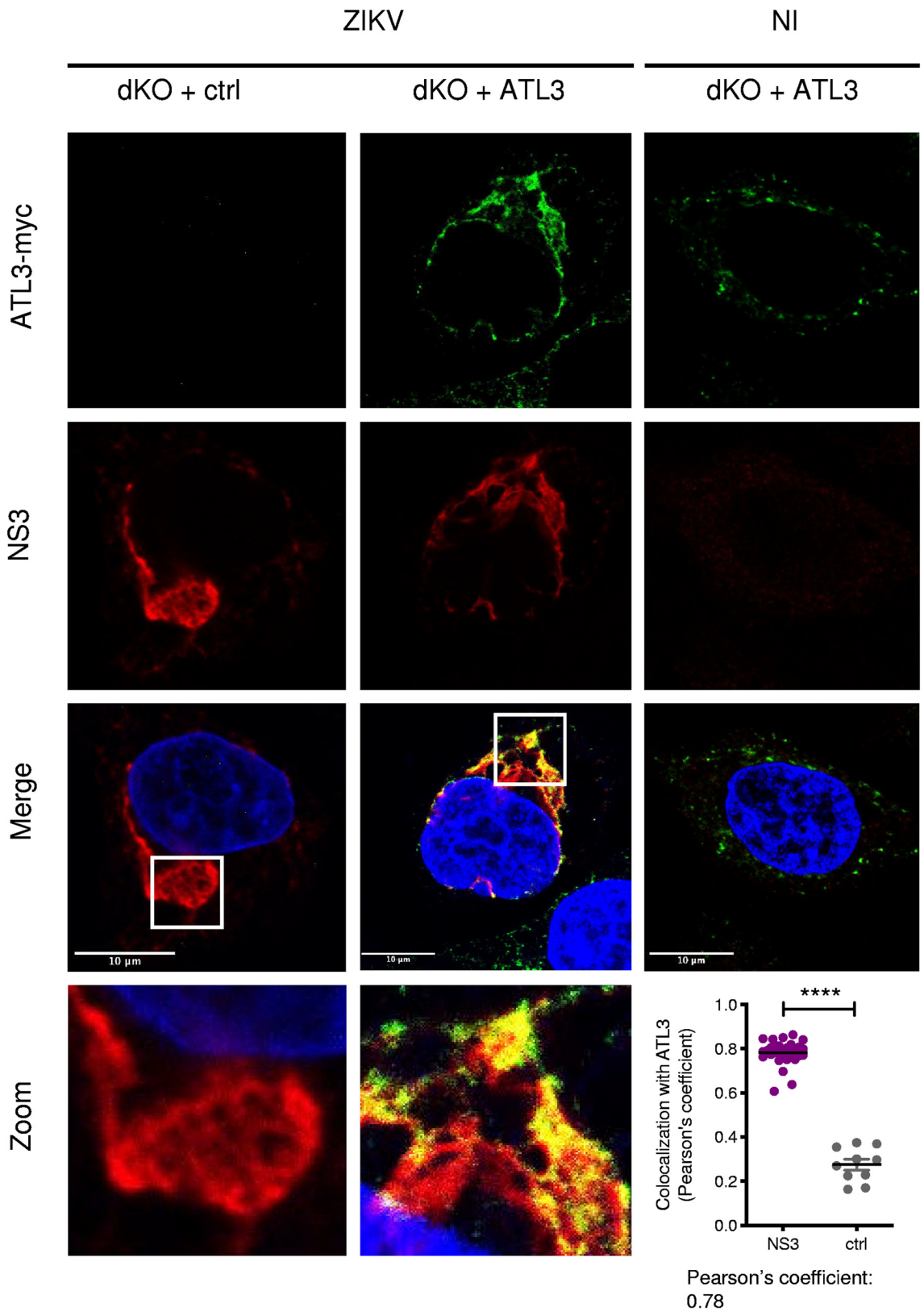

FIG 11 ATL3 colocalizes with NS3 in ZIKV-infected cells. HeLa dKO cells transduced with a control vector (dKO+ctrl) or stably expressing ATL3-myc (dKO+ATL3) were infected with ZIKV (MOI of 1) for 24 h. The cells were then fixed and stained for ATL3-myc (green) and NS3 (red). One field from a representative experiment is shown. Colocalization (Pearson's coefficient) was determined after deconvolution with Imaris software. At least 10 cells were plotted from three independent experiments. Statistical significance was determined using a *t* test. ****, $P < 0.0001$.

may be of interest to analyze how viral sensing and production of type I IFN is modulated by ATL and other ER-shaping proteins.

Hereditary sensory and autonomic neuropathies (HSAN) and spastic paraplegia (HSP) involve genes controlling the architecture of the ER and coding for proteins with RTN-like domain, namely, ARL6IP1, ATL1 and -3, FAM134B, REEP1, RTN2, and SPAST (33, 58). These mutations induce length-dependent axonopathy of projecting neurons. ZIKV infection during pregnancy leads to severe fetal abnormalities, including debilitating neuropathological outcomes and microcephaly (59). In adults, ZIKV infection can also result in peripheral neuropathy and meningoencephalitis (60). In some individuals, ZIKV accesses the central nervous system, where it infects neurons and neural progenitor cells (61). Experiments with cultured human neuroprogenitor stem cells, organoids, brain slices, and mouse inoculation studies demonstrated that ZIKV (i) targets neural progenitor cells of the cortex, neurons, microglial cells, and astrocytes, (ii) reduces cell proliferation and differentiation, and (iii) modulates inflammation and cell death (62–75). In ZIKV-Infected neurons, BP1/RIPK1/RIPK3 induces a transcriptional response that reprograms neuronal metabolism in a manner that further restricts viral replication (76). Future ZIKV infection experiments with cells from healthy individuals or from patients with HSP or HSAN should allow further characterization of the role of ATL and other ER-shaping proteins during ZIKV replication and will help to determine whether the virus may impact axonal growth.

MATERIALS AND METHODS

Cells, lentivectors, and viruses. HeLa cells (ATCC) and primary human adult dermal fibroblasts (HDFa; ATCC) were cultured in Dulbecco modified Eagle minimal essential medium supplemented with 10% fetal bovine serum and 1% penicillin-streptomycin at 37°C with 5% CO_2. HeLa cells stably expressing a fluorescent, calreticulin-based ER marker were established via transfection with pDsRed2-ER Vector (Clontech 632409) and G418 selection. HeLa knockouts for ATL2/ATL3 (dKO cells) were generated using a CRISPR strategy as previously described (42). HeLa cells stably expressing the mEmmerald Sec61β protein were generated by transduction with a lentivector expressing Sec61-mEmmerald. HeLa dKO cells were transduced with lentiviral vectors to stably express ATL3 WT, ATL3-myc, or ATL3KA.

ZIKV strains HD78788, PF13, NC14, and FG16 were previously described (8, 77–80). Virus stocks were produced on C6/36 cells, and titers were determined on Vero cells. Cells were seeded 1 day prior to infection and overlaid with ZIKV at the desired MOI in a final volume of 200 μl. After 2 h at 37°C, the inoculum was removed and replaced with fresh medium.

Plasmids. The Sec61-mEmmerald was amplified using PCR from the pUC_CMV-mEmmerald-Serc61 plasmid (Addgene, catalog no. 90992) and cloned into the pLV-EF1a-IRES-Puro Addgene (catalog no. 85132) using EcoRI to generate the pLV-EF1a-Sec61-mEmmerald-IRES-Puro plasmid. The pLVX-ATL3 is derived frompLVX-IRES-ZsGreen1 (Clontech, catalog no. 632187) and encodes WT AXL3. pLVX-ATL3-myc and pLVX-ATL3KA were generated as follows: restriction sites, Kozak sequence, and myc tag were added to ATL3 or ATL3KA from pGW1-ATL3 or pGW1-ATL3KA by PCR. The myc-ATL3 fragment was then inserted into pLVX-IRES-ZsGreen1.

Flow cytometry analysis. Cells were fixed with 4% paraformaldehyde (PFA) and permeabilized with 1% Triton X-100, followed by 30-min incubations with anti-E protein (4G2, purified from the ATCC hybridoma) and anti-mouse secondary antibodies. A Live/Dead Fixable Aqua dead cell stain kit (Thermo Fisher, catalog no. L34965) was used for cell death analysis. Samples were acquired with an Attune NxT flow cytometer (Becton Dickinson), and data were analyzed using FlowJo software. The gating strategy used to determine 4G2-positive cells is outlined in Fig. S6 in the supplemental material.

RNA measurement by RT-qPCR. Total RNA was extracted from cells using a QIAamp RNeasy extraction kit (Qiagen). RNA (500 ng) was used for cDNA synthesis using SuperScript II reverse transcriptase (Life Technologies) in an Eppendorf EP Mastercycler Gradient S thermocycler. The following primers were used to amplify viral cDNA as described previously (9): forward (AARTACACATACCARAACAAAGT GGT) and reverse (TCCRCTCCCYCTYTGGTCTTG). cDNAs corresponding to cellular transcripts were amplified using the following primers: ATL1, forward (TTG GCT ACT TAG TCC CGA GAG) and reverse (TGT AAC ATG GAT TTG GGA TGT GG); ATL2, forward (AGT AGT GGT ATC TGT GGC AGG) and reverse (CAC CTC GCC ATG TAA AGC CT); ATL3, forward (ACA GCC AGT CAA CTG TGA AAG) and reverse (CCA GAC GAC CGT ATT CTG TGA); DDOST, forward (GAG ACT CAT TCG CTT TTC TTC CG) and reverse (CTC CAA AAT CTT CTA CCG AAG GG); and RLP13, forward (AGG CAT CAA CAT TTC TGG CA) and reverse (CCA TCC GCT TTT TCT TGT CG).

cDNA amplification was performed by qPCR using 500 nM concentrations of each primer, 25 ng of cDNA, and 10 μl of SYBR green. An activation step of 15 min at 95°C was followed by 40 amplification cycles of 95°C for 15 s, 60°C for 20 s, and 72°C for 30 s. The levels of viral RNA or cellular transcripts were normalized to GAPDH (glyceraldehyde-3-phosphate dehydrogenase) or to RLP13.

Transmission electron microscopy. HeLa siSCR or HeLa siATL1/2/3 cells were fixed for 24 h in 4% PFA and 1% glutaraldehyde (Sigma) in 0.1 M phosphate buffer (pH 7.2). Cells were washed in PBS and postfixed with 2% osmium tetroxide (Agar Scientific) for 1 h. The cells were fully dehydrated in a graded

series of ethanol solutions and propylene oxide. The impregnation step was performed with a mixture of (1:1) propylene oxide/Epon resin (Sigma) and left overnight in pure resin. The cells were then embedded in resin blocks, which were allowed to polymerize for 48 h at 60°C. Ultrathin sections (70 nm) of blocks were obtained with a Leica EM UC7 ultramicrotome (Wetzlar). Sections were stained with 5% uranyl acetate (Agar Scientific) and 5% lead citrate (Sigma), and observations were made with a JEOL 1011 transmission electron microscope.

Western blotting. Cells were lysed in 1% radioimmunoprecipitation assay (RIPA) buffer in the presence of protease inhibitor cocktail (Sigma, catalog no. R0278), and 10 to 20 μg of protein lysates was loaded into 12% Bis-Tris SDS-PAGE gels. The following antibodies were used: anti-ATL3 (Atlas Antibodies, catalog no. HPA065702) and mouse anti-cMyc (Fisher Scientific, catalog no. 10416023). DyLight-coupled secondary antibodies (Thermo Fisher) were used for protein detection on a Li-Cor Odyssey imaging system.

Confocal microscopy and structured illumination microscopy. For ER morphology analysis, HeLa WT, dKO, dKO+ATL3, and dKO+ATL3KA cells stably expressing the red ER-tracker were plated on coverslips and fixed with 4% PFA for 10 min at room temperature. The coverslips were then mounted on slides with Fluoromount-G with DAPI (Thermo Fisher Scientific, catalog no. 00-4959-52). The cells were analyzed using confocal microscopy (Leica SP5 HyD inverted), a 63× oil immersion objective, and LAS AF software. The ER-tracker signal was analyzed and normalized to the selected area of the cells after background subtraction using ImageJ software.

Sec61β relocation and viral replication site: HeLa WT or dKO cells stably expressing mEmmerald-Sec61β protein were plated on coverslips in 24-well plates and challenged with ZIKV (MOI of 1) for 24 h. The cells were fixed 30 min at room temperature with 4% PFA, permeabilized with Triton 1% for 10 min blocked with 1% PBS-BSA for 30 min, and stained for viral E protein using 4G2 antibody (1 μg/ml) for 45 and 30 min with an anti-mouse secondary antibody. The coverslips were mounted on slides using Fluoromount-G with DAPI and analyzed using confocal microscopy or super-resolution microscopy (structured illumination microscopy [SIM]; Zeiss LSM 780-Elyra PS.1). A Plan Apo 63×/1.4 oil objective with a 1.518 refractive index oil (Zeiss) and an EMCCD Andor Ixon 887 1K camera were used. Fifteen images per plane per channel (five phases, three angles) were acquired to obtaine SIM images. The SIM images were processed with Zen software and then aligned with Zen using 100-nm TetraSpeck microspheres (Thermo Fisher Scientific) embedded under the same conditions as the sample. The acquired pictures were analyzed using ImageJ software.

For colocalization of ATL3-myc and NS-HA proteins, HeLa dKO or HeLa dKO+ATL3-myc cells were transfected with plasmids coding for individual viral NS-HA proteins with TurboFect (Thermo Fisher Scientific, catalog no. 0531). After 40 h, the cells were fixed 30 min at room temperature with 4% PFA, permeabilized with Triton 1% for 10 min at room temperature, blocked with 1% PBS-BSA for 30 min at room temperature, and stained with rat anti-HA antibody 3F10 (Roche, catalog no. 11867423001) and mouse anti-cMyc (Fisher Scientific, catalog no. 10416023) antibody. For colocalization of ATL3 and NS3 in the context of viral infections, HeLa dKO or dKO+ATL3-myc cells were infected with ZIKV at an MOI of 1 for 24 h and stained with a rabbit anti-NS3 antibody kindly provided by Andres Merits (81). The cells were analyzed using confocal microscopy (Leica SP5 HyD inverted), a 63× oil immersion objective, and LAS AF software. The acquired pictures were deconvoluted using Huygens software, and the colocalization was quantified with Imaris software.

Time-lapse microscopy. HeLa cells stably expressing Sec61β-mEmmerald were plated in Hi-Q4 microdishes (10,000 cells per chamber; Ibidi). The following day, the cells were infected with ZIKV (MOI of 1). Transmission and fluorescence images were taken every 5 min for up to 48 h using a Nikon Biostation IMQ, with three fields captured simultaneously for each condition. The images were analyzed with Fiji software.

ZIKV cell attachment and entry. HeLa cells were plated in 24-well plates (50,000 cells/well) with at least four wells/condition. The cells were challenged with ZIKV (MOI of 1 or 10) for 1 h at 4°C. The viral input was removed, and the cells were washed with PBS to remove the unbound particles. Half of the wells were treated with PBS-EDTA to gently detach the cells. The other half of the wells were kept at 37°C for 2 h to allow viral endocytosis/fusion. The cells were then treated with trypsin for 30 min at 37°C to remove the bound particles. The cells were pelleted for lysis, RNA extraction, and RT-qPCR to quantify the viral RNA.

Reporter viral RNA transfection and replication kinetics. To assess ZIKV RNA amplification, HeLa WT and dKO cells were transfected with a genomic viral RNA expressing *Renilla* luciferase (R-Luc), kindly provided by Pei-Yong Shi (University of Texas Medical Branch) (43). The ZIKV R-Luc reporter viral RNA was generated as previously described (43). A total of 3×10^4 cells were plated on a 48-well plate and transfected with 100 ng of RNA using Lipofectamine MessengerMax (Thermo Fisher). At the indicated time points, cells were lysed with 1× *Renilla* lysis buffer (Promega). The lysates were kept at −20°C until all of the samples were collected. Viral replication was measured with the *Renilla* luciferase assay (E2820; Promega) on a TriStar2 LB942 microplate reader (Berthold Technologies).

Coimmunoprecipitation. 293T cells were plated in 10-cm dishes and transfected with 7.5-μg portions of each indicated plasmid. After 24 h, the cells were washed and collected with a scrapper, and the pellets were lysed for 30 min in cold immunoprecipitation lysis buffer supplemented with Halt protease and phosphatase inhibitor cocktail (Thermo Fisher Scientific) and cleared by centrifugation (15 min at 6,000 × *g*). Supernatants were incubated overnight at 4°C with anti-HA magnetic beads (catalog no. 88837; Thermo Fisher Scientific). Beads were washed three times with BO15 buffer (20 mM Tris-HCl [pH 7.4], 150 mM NaCl, 5 mM $MgCl_2$, 10% glycerol, 0.5 mM EDTA, 0.05% Triton, 0.1% Tween 20). The retained complexes were eluted twice with HA peptide (400 μg/ml; Roche, catalog no. 11666975001)

for 30 min at room temperature. Samples were then subjected to immunoblotting with the following antibodies: mouse anti-GAPDH (SC-47724, 1:5,000; Santa Cruz), rabbit anti-HA (catalog no. 3724, 1:5,000; Cell Signaling Technology), and mouse anti-Myc (catalog no. 2276S, 1:2,000; Cell Signaling Technology). The signals were acquired by using a Fusion Fx camera (VILBERT Lourmat).

SUPPLEMENTAL MATERIAL

Supplemental material for this article may be found at https://doi.org/10.1128/JVI.01047-19.

SUPPLEMENTAL FILE 1, AVI file, 7 MB.

SUPPLEMENTAL FILE 2, AVI file, 6.2 MB.

SUPPLEMENTAL FILE 3, PDF file, 0.03 MB.

ACKNOWLEDGMENTS

We thank members of the Virus and Immunity Unit for discussions and assistance, Pei-Yong Shi (University of Texas Medical Branch) for the kind gift of the infectious ZIKV clone, and Andrès Merits (Institute of Technology, University of Tartu, Tartu, Estonia) for the kind gift of the anti-NS3 antibody. We also thank the World Reference Center for Emerging Viruses and Arboviruses (University of Texas Medical Branch, Galveston, TX) for the ZIKV luciferase clone.

Work in the O.S. lab is funded by Institut Pasteur, ANRS, Sidaction, the Vaccine Research Institute (ANR-10-LABX-77), Labex IBEID (ANR-10-LABX-62-IBEID), TIMTAMDEN ANR-14-CE14-0029, CHIKV-Viro-Immuno ANR-14-CE14-0015-01, and the Gilead HIV cure program. Work in the A.A. lab is funded by ANR (ANR-15-CE15-00029 ZIKAHOST). This study was supported in part by the Intramural Research Program of the NINDS, NIH. UTechS PBI is part of the France–BioImaging infrastructure network (FBI) supported by the French National Research Agency (ANR-10–INSB–04; Investments for the Future) and acknowledges support from ANR/FBI and the Région Ile-de-France (program "Domaine d'Intérêt Majeur-Malinf") for the use of the Zeiss LSM 780 Elyra PS1 microscope. M.M.R. is supported by the Pasteur-Paris University International PhD program.

B.M., N.J., P.R., C.B., A.A., and O.S. designed the experimental strategy. B.M., M.M.R., M.-L.H., S.S.-A., J.B.-G., Q.N., J.B., F.P., C.M., S.A., M.C., and A.S. designed and performed experiments. P.-P.Z. and C.B. provided vital materials and expert advice. B.M. and O.S. wrote the manuscript. All authors agreed on the final version and declare no competing interests.

REFERENCES

1. Weaver SC, Costa F, Garcia-Blanco MA, Ko AI, Ribeiro GS, Saade G, Shi PY, Vasilakis N. 2016. Zika virus: history, emergence, biology, and prospects for control. Antiviral Res 130:69–80. https://doi.org/10.1016/j.antiviral.2016.03.010.
2. Pierson TC, Diamond MS. 2018. The emergence of Zika virus and its new clinical syndromes. Nature 560:573–581. https://doi.org/10.1038/s41586-018-0446-y.
3. Liu ZY, Shi WF, Qin CF. 2019. The evolution of Zika virus from Asia to the Americas. Nat Rev Microbiol 17:131. https://doi.org/10.1038/s41579-018-0134-9.
4. da Silva S, Oliveira Silva Martins D, Jardim A. 2018. A review of the ongoing research on Zika Virus treatment. Viruses 10:255. https://doi.org/10.3390/v10050255.
5. Abbink P, Stephenson KE, Barouch DH. 2018. Zika virus vaccines. Nat Rev Microbiol 16:594–600. https://doi.org/10.1038/s41579-018-0039-7.
6. Lee I, Bos S, Li G, Wang S, Gadea G, Despres P, Zhao RY. 2018. Probing molecular insights into Zika virus(–)host interactions. Viruses 10:233. https://doi.org/10.3390/v10050233.
7. Richner JM, Diamond MS. 2018. Zika virus vaccines: immune response, current status, and future challenges. Curr Opin Immunol 53:130–136. https://doi.org/10.1016/j.coi.2018.04.024.
8. Hamel R, Dejarnac O, Wichit S, Ekchariyawat P, Neyret A, Luplertlop N, Perera-Lecoin M, Surasombatpattana P, Talignani L, Thomas F, Cao-Lormeau V-M, Choumet V, Briant L, Desprès P, Amara A, Yssel H, Missé D. 2015. Biology of Zika virus infection in human skin cells. J Virol 89:8880–8896. https://doi.org/10.1128/JVI.00354-15.
9. Meertens L, Labeau A, Dejarnac O, Cipriani S, Sinigaglia L, Bonnet-Madin L, Le Charpentier T, Hafirassou ML, Zamborlini A, Cao-Lormeau VM, Coulpier M, Misse D, Jouvenet N, Tabibiazar R, Gressens P, Schwartz O, Amara A. 2017. Axl mediates ZIKA virus entry in human glial cells and modulates innate immune responses. Cell Rep 18:324–333. https://doi.org/10.1016/j.celrep.2016.12.045.
10. Pierson TC, Kielian M. 2013. Flaviviruses: braking the entering. Curr Opin Virol 3:3–12. https://doi.org/10.1016/j.coviro.2012.12.001.
11. Gillespie LK, Hoenen A, Morgan G, Mackenzie JM. 2010. The endoplasmic reticulum provides the membrane platform for biogenesis of the flavivirus replication complex. J Virol 84:10438–10447. https://doi.org/10.1128/JVI.00986-10.
12. Neufeldt CJ, Cortese M, Acosta EG, Bartenschlager R. 2018. Rewiring cellular networks by members of the *Flaviviridae* family. Nat Rev Microbiol 16:125–142. https://doi.org/10.1038/nrmicro.2017.170.
13. Blanchard E, Roingeard P. 2015. Virus-induced double-membrane vesicles. Cell Microbiol 17:45–50. https://doi.org/10.1111/cmi.12372.
14. Paul D, Bartenschlager R. 2015. *Flaviviridae* replication organelles: oh, what a tangled web we weave. Annu Rev Virol 2:289–310. https://doi.org/10.1146/annurev-virology-100114-055007.
15. Ravindran MS, Bagchi P, Cunningham CN, Tsai B. 2016. Opportunistic intruders: how viruses orchestrate ER functions to infect cells. Nat Rev Microbiol 14:407–420. https://doi.org/10.1038/nrmicro.2016.60.
16. Saeedi BJ, Geiss BJ. 2013. Regulation of flavivirus RNA synthesis and capping. Wiley Interdiscip Rev RNA 4:723–735. https://doi.org/10.1002/wrna.1191.

17. Klema VJ, Padmanabhan R, Choi KH. 2015. Flaviviral replication complex: coordination between RNA synthesis and 5′-RNA capping. Viruses 7:4640–4656. https://doi.org/10.3390/v7082837.
18. Cortese M, Goellner S, Acosta EG, Neufeldt CJ, Oleksiuk O, Lampe M, Haselmann U, Funaya C, Schieber N, Ronchi P, Schorb M, Pruunsild P, Schwab Y, Chatel-Chaix L, Ruggieri A, Bartenschlager R. 2017. Ultrastructural characterization of Zika virus replication factories. Cell Rep 18:2113–2123. https://doi.org/10.1016/j.celrep.2017.02.014.
19. Rossignol ED, Peters KN, Connor JH, Bullitt E. 2017. Zika virus induced cellular remodeling. Cell Microbiol. https://doi.org/10.1111/cmi.12740.
20. Aktepe TE, Mackenzie JM. 2018. Shaping the flavivirus replication complex: it is curvaceous!. Cell Microbiol 20:e12884. https://doi.org/10.1111/cmi.12884.
21. Blázquez A-B, Escribano-Romero E, Merino-Ramos T, Saiz J-C, Martín-Acebes MA. 2014. Stress responses in flavivirus-infected cells: activation of unfolded protein response and autophagy. Front Microbiol 5:266. https://doi.org/10.3389/fmicb.2014.00266.
22. Tan Z, Zhang W, Sun J, Fu Z, Ke X, Zheng C, Zhang Y, Li P, Liu Y, Hu Q, Wang H, Zheng Z. 2018. ZIKV infection activates the IRE1-XBP1 and ATF6 pathways of unfolded protein response in neural cells. J Neuroinflammation 15:275. https://doi.org/10.1186/s12974-018-1311-5.
23. Monel B, Compton AA, Bruel T, Amraoui S, Burlaud-Gaillard J, Roy N, Guivel-Benhassine F, Porrot F, Génin P, Meertens L, Sinigaglia L, Jouvenet N, Weil R, Casartelli N, Demangel C, Simon-Lorière E, Moris A, Roingeard P, Amara A, Schwartz O. 2017. Zika virus induces massive cytoplasmic vacuolization and paraptosis-like death in infected cells. EMBO J 36:1653–1668. https://doi.org/10.15252/embj.201695597.
24. Voeltz GK, Prinz WA, Shibata Y, Rist JM, Rapoport TA. 2006. A class of membrane proteins shaping the tubular endoplasmic reticulum. Cell 124:573–586. https://doi.org/10.1016/j.cell.2005.11.047.
25. Goyal U, Blackstone C. 2013. Untangling the web: mechanisms underlying ER network formation. Biochim Biophys Acta 1833:2492–2498. https://doi.org/10.1016/j.bbamcr.2013.04.009.
26. Wang S, Tukachinsky H, Romano FB, Rapoport TA. 2016. Cooperation of the ER-shaping proteins atlastin, lunapark, and reticulons to generate a tubular membrane network. Elife 5:e18605. https://doi.org/10.7554/eLife.18605.
27. Hu J, Shibata Y, Zhu PP, Voss C, Rismanchi N, Prinz WA, Rapoport TA, Blackstone C. 2009. A class of dynamin-like GTPases involved in the generation of the tubular ER network. Cell 138:549–561. https://doi.org/10.1016/j.cell.2009.05.025.
28. Orso G, Pendin D, Liu S, Tosetto J, Moss TJ, Faust JE, Micaroni M, Egorova A, Martinuzzi A, McNew JA, Daga A. 2009. Homotypic fusion of ER membranes requires the dynamin-like GTPase atlastin. Nature 460:978–983. https://doi.org/10.1038/nature08280.
29. Rismanchi N, Soderblom C, Stadler J, Zhu PP, Blackstone C. 2008. Atlastin GTPases are required for Golgi apparatus and ER morphogenesis. Hum Mol Genet 17:1591–1604. https://doi.org/10.1093/hmg/ddn046.
30. Blackstone C, O'Kane CJ, Reid E. 2011. Hereditary spastic paraplegias: membrane traffic and the motor pathway. Nat Rev Neurosci 12:31. https://doi.org/10.1038/nrn2946.
31. Evans K, Keller C, Pavur K, Glasgow K, Conn B, Lauring B. 2006. Interaction of two hereditary spastic paraplegia gene products, spastin and atlastin, suggests a common pathway for axonal maintenance. Proc Natl Acad Sci U S A 103:10666–10671. https://doi.org/10.1073/pnas.0510863103.
32. Sanderson CM, Connell JW, Edwards TL, Bright NA, Duley S, Thompson A, Luzio JP, Reid E. 2006. Spastin and atlastin, two proteins mutated in autosomal-dominant hereditary spastic paraplegia, are binding partners. Hum Mol Genet 15:307–318. https://doi.org/10.1093/hmg/ddi447.
33. Park SH, Zhu PP, Parker RL, Blackstone C. 2010. Hereditary spastic paraplegia proteins REEP1, spastin, and atlastin-1 coordinate microtubule interactions with the tubular ER network. J Clin Invest 120:1097–1110. https://doi.org/10.1172/JCI40979.
34. Montenegro G, Rebelo AP, Connell J, Allison R, Babalini C, D'Aloia M, Montieri P, Schüle R, Ishiura H, Price J, Strickland A, Gonzalez MA, Baumbach-Reardon L, Deconinck T, Huang J, Bernardi G, Vance JM, Rogers MT, Tsuji S, De Jonghe P, Pericak-Vance MA, Schöls L, Orlacchio A, Reid E, Züchner S. 2012. Mutations in the ER-shaping protein reticulon 2 cause the axon-degenerative disorder hereditary spastic paraplegia type 12. J Clin Invest 122:538–544. https://doi.org/10.1172/JCI60560.
35. Zhao J, Hedera P. 2013. Hereditary spastic paraplegia-causing mutations in atlastin-1 interfere with BMPRII trafficking. Mol Cell Neurosci 52:87–96. https://doi.org/10.1016/j.mcn.2012.10.005.
36. Willkomm L, Heredia R, Hoffmann K, Wang H, Voit T, Hoffman EP, Cirak S. 2016. Homozygous mutation in atlastin GTPase 1 causes recessive hereditary spastic paraplegia. J Hum Genet 61:571–573. https://doi.org/10.1038/jhg.2016.6.
37. Aktepe TE, Liebscher S, Prier JE, Simmons CP, Mackenzie JM. 2017. The host protein reticulon 3.1A is utilized by flaviviruses to facilitate membrane remodeling. Cell Rep 21:1639–1654. https://doi.org/10.1016/j.celrep.2017.10.055.
38. Savidis G, McDougall WM, Meraner P, Perreira JM, Portmann JM, Trincucci G, John SP, Aker AM, Renzette N, Robbins DR, Guo Z, Green S, Kowalik TF, Brass AL. 2016. Identification of Zika virus and dengue virus dependency factors using functional genomics. Cell Rep 16:232–246. https://doi.org/10.1016/j.celrep.2016.06.028.
39. Marceau CD, Puschnik AS, Majzoub K, Ooi YS, Brewer SM, Fuchs G, Swaminathan K, Mata MA, Elias JE, Sarnow P, Carette JE. 2016. Genetic dissection of *Flaviviridae* host factors through genome-scale CRISPR screens. Nature 535:159–163. https://doi.org/10.1038/nature18631.
40. Hafirassou ML, Meertens L, Umana-Diaz C, Labeau A, Dejarnac O, Bonnet-Madin L, Kummerer BM, Delaugerre C, Roingeard P, Vidalain PO, Amara A. 2017. A global interactome map of the dengue virus NS1 identifies virus restriction and dependency host factors. Cell Rep 21:3900–3913. https://doi.org/10.1016/j.celrep.2017.11.094.
41. Petrova E, Gracias S, Beauclair G, Tangy F, Jouvenet N. 2019. Uncovering flavivirus host dependency factors through a genome-wide gain-of-function screen. Viruses 11:68. https://doi.org/10.3390/v11010068.
42. Zhao G, Zhu PP, Renvoise B, Maldonado-Baez L, Park SH, Blackstone C. 2016. Mammalian knock out cells reveal prominent roles for atlastin GTPases in ER network morphology. Exp Cell Res 349:32–44. https://doi.org/10.1016/j.yexcr.2016.09.015.
43. Shan C, Xie X, Muruato AE, Rossi SL, Roundy CM, Azar SR, Yang Y, Tesh RB, Bourne N, Barrett AD, Vasilakis N, Weaver SC, Shi PY. 2016. An infectious cDNA clone of Zika virus to study viral virulence, mosquito transmission, and antiviral inhibitors. Cell Host Microbe 19:891–900. https://doi.org/10.1016/j.chom.2016.05.004.
44. Coyaud E, Ranadheera C, Cheng D, Goncalves J, Dyakov BJA, Laurent EMN, St-Germain J, Pelletier L, Gingras AC, Brumell JH, Kim PK, Safronetz D, Raught B. 2018. Global interactomics uncovers extensive organellar targeting by Zika virus. Mol Cell Proteomics 17:2242–2255. https://doi.org/10.1074/mcp.TIR118.000800.
45. Scaturro P, Stukalov A, Haas DA, Cortese M, Draganova K, Płaszczyca A, Bartenschlager R, Götz M, Pichlmair A. 2018. An orthogonal proteomic survey uncovers novel Zika virus host factors. Nature 561:253–257. https://doi.org/10.1038/s41586-018-0484-5.
46. Shah PS, Link N, Jang GM, Sharp PP, Zhu T, Swaney DL, Johnson JR, Von Dollen J, Ramage HR, Satkamp L, Newton B, Huttenhain R, Petit MJ, Baum T, Everitt A, Laufman O, Tassetto M, Shales M, Stevenson E, Iglesias GN, Shokat L, Tripathi S, Balasubramaniam V, Webb LG, Aguirre S, Willsey AJ, Garcia-Sastre A, Pollard KS, Cherry S, Gamarnik AV, Marazzi I, Taunton J, Fernandez-Sesma A, Bellen HJ, Andino R, Krogan NJ. 2018. Comparative flavivirus-host protein interaction mapping reveals mechanisms of dengue and Zika virus pathogenesis. Cell 175:1931–1945 e18. https://doi.org/10.1016/j.cell.2018.11.028.
47. Tang WF, Yang SY, Wu BW, Jheng JR, Chen YL, Shih CH, Lin KH, Lai HC, Tang P, Horng JT. 2007. Reticulon 3 binds the 2C protein of enterovirus 71 and is required for viral replication. J Biol Chem 282:5888–5898. https://doi.org/10.1074/jbc.M611145200.
48. Diaz A, Wang X, Ahlquist P. 2010. Membrane-shaping host reticulon proteins play crucial roles in viral RNA replication compartment formation and function. Proc Natl Acad Sci U S A 107:16291–16296. https://doi.org/10.1073/pnas.1011105107.
49. Wu MJ, Ke PY, Hsu JT, Yeh CT, Horng JT. 2014. Reticulon 3 interacts with NS4B of the hepatitis C virus and negatively regulates viral replication by disrupting NS4B self-interaction. Cell Microbiol 16:1603–1618. https://doi.org/10.1111/cmi.12318.
50. Westrate LM, Lee JE, Prinz WA, Voeltz GK. 2015. Form follows function: the importance of endoplasmic reticulum shape. Annu Rev Biochem 84:791–811. https://doi.org/10.1146/annurev-biochem-072711-163501.
51. Zhu PP, Patterson A, Lavoie B, Stadler J, Shoeb M, Patel R, Blackstone C. 2003. Cellular localization, oligomerization, and membrane association of the hereditary spastic paraplegia 3A (SPG3A) protein atlastin. J Biol Chem 278:49063–49071. https://doi.org/10.1074/jbc.M306702200.
52. Gladwyn-Ng I, Cordon-Barris L, Alfano C, Creppe C, Couderc T, Morelli G, Thelen N, America M, Bessieres B, Encha-Razavi F, Bonniere M, Suzuki IK, Flamand M, Vanderhaeghen P, Thiry M, Lecuit M, Nguyen L. 2018. Stress-

induced unfolded protein response contributes to Zika virus-associated microcephaly. Nat Neurosci 21:63–71. https://doi.org/10.1038/s41593-017-0038-4.
53. Niu L, Ma T, Yang F, Yan B, Tang X, Yin H, Wu Q, Huang Y, Yao ZP, Wang J, Guo Y, Hu J. 2019. Atlastin-mediated membrane tethering is critical for cargo mobility and exit from the endoplasmic reticulum. Proc Natl Acad Sci U S A 116:14029–14038. https://doi.org/10.1073/pnas.1908409116.
54. Suthar MS, Aguirre S, Fernandez-Sesma A. 2013. Innate immune sensing of flaviviruses. PLoS Pathog 9:e1003541. https://doi.org/10.1371/journal.ppat.1003541.
55. Green AM, Beatty PR, Hadjilaou A, Harris E. 2014. Innate immunity to dengue virus infection and subversion of antiviral responses. J Mol Biol 426:1148–1160. https://doi.org/10.1016/j.jmb.2013.11.023.
56. Kim J-A, Seong R-K, Son SW, Shin OS. 2018. Insights into ZIKV-mediated innate immune responses in human dermal fibroblasts and epidermal keratinocytes. J Invest Dermatol. https://doi.org/10.1016/j.jid.2018.07.038.
57. Chazal M, Beauclair G, Gracias S, Najburg V, Simon-Lorière E, Tangy F, Komarova AV, Jouvenet N. 2018. RIG-I recognizes the 5′ region of dengue and Zika virus genomes. Cell Rep 24:320–328. https://doi.org/10.1016/j.celrep.2018.06.047.
58. Hubner CA, Kurth I. 2014. Membrane-shaping disorders: a common pathway in axon degeneration. Brain 137:3109–3121. https://doi.org/10.1093/brain/awu287.
59. Coyne CB, Lazear HM. 2016. Zika virus: reigniting the TORCH. Nat Rev Microbiol 14:707–715. https://doi.org/10.1038/nrmicro.2016.125.
60. Hygino da Cruz LC, Jr, Nascimento OJM, Lopes F, da Silva I. 2018. Neuroimaging findings of Zika virus-associated neurologic complications in adults. AJNR 39:1967–1974. https://doi.org/10.3174/ajnr.A5649.
61. Miner JJ, Diamond MS. 2017. Zika virus pathogenesis and tissue tropism. Cell Host Microbe 21:134–142. https://doi.org/10.1016/j.chom.2017.01.004.
62. Dang J, Tiwari SK, Lichinchi G, Qin Y, Patil VS, Eroshkin AM, Rana TM. 2016. Zika virus depletes neural progenitors in human cerebral organoids through activation of the innate immune receptor TLR3. Cell Stem Cell 19:258–265. https://doi.org/10.1016/j.stem.2016.04.014.
63. Garcez PP, Loiola EC, Madeiro da Costa R, Higa LM, Trindade P, Delvecchio R, Nascimento JM, Brindeiro R, Tanuri A, Rehen SK. 2016. Zika virus impairs growth in human neurospheres and brain organoids. Science 352:816–818. https://doi.org/10.1126/science.aaf6116.
64. Retallack H, Di Lullo E, Arias C, Knopp KA, Laurie MT, Sandoval-Espinosa C, Mancia Leon WR, Krencik R, Ullian EM, Spatazza J, Pollen AA, Mandel-Brehm C, Nowakowski TJ, Kriegstein AR, DeRisi JL. 2016. Zika virus cell tropism in the developing human brain and inhibition by azithromycin. Proc Natl Acad Sci U S A 113:14408–14413. https://doi.org/10.1073/pnas.1618029113.
65. Simonin Y, Loustalot F, Desmetz C, Foulongne V, Constant O, Fournier-Wirth C, Leon F, Moles JP, Goubaud A, Lemaitre JM, Maquart M, Leparc-Goffart I, Briant L, Nagot N, Van de Perre P, Salinas S. 2016. Zika virus strains potentially display different infectious profiles in human neural cells. EBioMedicine 12:161–169. https://doi.org/10.1016/j.ebiom.2016.09.020.
66. Souza BS, Sampaio GL, Pereira CS, Campos GS, Sardi SI, Freitas LA, Figueira CP, Paredes BD, Nonaka CK, Azevedo CM, Rocha VP, Bandeira AC, Mendez-Otero R, Dos Santos RR, Soares MB. 2016. Zika virus infection induces mitosis abnormalities and apoptotic cell death of human neural progenitor cells. Sci Rep 6:39775. https://doi.org/10.1038/srep39775.
67. Tang H, Hammack C, Ogden SC, Wen Z, Qian X, Li Y, Yao B, Shin J, Zhang F, Lee EM, Christian KM, Didier RA, Jin P, Song H, Ming GL. 2016. Zika virus infects human cortical neural progenitors and attenuates their growth. Cell Stem Cell 18:587–590. https://doi.org/10.1016/j.stem.2016.02.016.
68. Anfasa F, Siegers JY, van der Kroeg M, Mumtaz N, Stalin Raj V, de Vrij FMS, Widagdo W, Gabriel G, Salinas S, Simonin Y, Reusken C, Kushner SA, Koopmans MPG, Haagmans B, Martina BEE, van Riel D. 2017. Phenotypic differences between Asian and African lineage Zika viruses in human neural progenitor cells. mSphere 2. https://doi.org/10.1128/mSphere.00292-17.
69. Garcez PP, Nascimento JM, de Vasconcelos JM, Madeiro da Costa R, Delvecchio R, Trindade P, Loiola EC, Higa LM, Cassoli JS, Vitória G, Sequeira PC, Sochacki J, Aguiar RS, Fuzii HT, de Filippis AMB, da Silva Gonçalves Vianez Júnior JL, Tanuri A, Martins-de-Souza D, Rehen SK. 2017. Zika virus disrupts molecular fingerprinting of human neurospheres. Sci Rep 7:40780. https://doi.org/10.1038/srep40780.
70. Lin MY, Wang YL, Wu WL, Wolseley V, Tsai MT, Radic V, Thornton ME, Grubbs BH, Chow RH, Huang IC. 2017. Zika virus infects intermediate progenitor cells and post-mitotic committed neurons in human fetal brain tissues. Sci Rep 7:14883. https://doi.org/10.1038/s41598-017-13980-2.
71. Lum FM, Low DK, Fan Y, Tan JJ, Lee B, Chan JK, Renia L, Ginhoux F, Ng LF. 2017. Zika virus infects human fetal brain microglia and induces inflammation. Clin Infect Dis 64:914–920. https://doi.org/10.1093/cid/ciw878.
72. Olmo IG, Carvalho TG, Costa VV, Alves-Silva J, Ferrari CZ, Izidoro-Toledo TC, da Silva JF, Teixeira AL, Souza DG, Marques JT, Teixeira MM, Vieira LB, Ribeiro FM. 2017. Zika virus promotes neuronal cell death in a non-cell autonomous manner by triggering the release of neurotoxic factors. Front Immunol 8:1016. https://doi.org/10.3389/fimmu.2017.01016.
73. Rosenfeld AB, Doobin DJ, Warren AL, Racaniello VR, Vallee RB. 2017. Replication of early and recent Zika virus isolates throughout mouse brain development. Proc Natl Acad Sci U S A 114:12273–12278. https://doi.org/10.1073/pnas.1714624114.
74. He Z, Chen J, Zhu X, An S, Dong X, Yu J, Zhang S, Wu Y, Li G, Zhang Y, Wu J, Li M. 2018. NLRP3 inflammasome activation mediates Zika virus-associated inflammation. J Infect Dis 217:1942–1951. https://doi.org/10.1093/infdis/jiy129.
75. Muffat J, Li Y, Omer A, Durbin A, Bosch I, Bakiasi G, Richards E, Meyer A, Gehrke L, Jaenisch R. 2018. Human induced pluripotent stem cell-derived glial cells and neural progenitors display divergent responses to Zika and dengue infections. Proc Natl Acad Sci U S A 115:7117–7122. https://doi.org/10.1073/pnas.1719266115.
76. Daniels BP, Kofman SB, Smith JR, Norris GT, Snyder AG, Kolb JP, Gao X, Locasale JW, Martinez J, Gale M, Jr, Loo YM, Oberst A. 2019. The nucleotide sensor ZBP1 and kinase RIPK3 induce the enzyme IRG1 to promote an antiviral metabolic state in neurons. Immunity 50:64–76. https://doi.org/10.1016/j.immuni.2018.11.017.
77. Hamel R, Ferraris P, Wichit S, Diop F, Talignani L, Pompon J, Garcia D, Liegeois F, Sall AA, Yssel H, Misse D. 2017. African and Asian Zika virus strains differentially induce early antiviral responses in primary human astrocytes. Infect Genet Evol 49:134–137. https://doi.org/10.1016/j.meegid.2017.01.015.
78. Barba-Spaeth G, Dejnirattisai W, Rouvinski A, Vaney MC, Medits I, Sharma A, Simon-Loriere E, Sakuntabhai A, Cao-Lormeau VM, Haouz A, England P, Stiasny K, Mongkolsapaya J, Heinz FX, Screaton GR, Rey FA. 2016. Structural basis of potent Zika-dengue virus antibody cross-neutralization. Nature 536:48–53. https://doi.org/10.1038/nature18938.
79. Chouin-Carneiro T, Vega-Rua A, Vazeille M, Yebakima A, Girod R, Goindin D, Dupont-Rouzeyrol M, Lourenço-de-Oliveira R, Failloux A-B. 2016. Differential susceptibilities of *Aedes aegypti* and *Aedes albopictus* from the Americas to Zika virus. PLoS Negl Trop Dis 10:e0004543. https://doi.org/10.1371/journal.pntd.0004543.
80. Fritzell C, Raude J, Kazanji M, Flamand C. 2018. Emerging trends of Zika apprehension in an epidemic setting. PLoS Negl Trop Dis 12:e0006167. https://doi.org/10.1371/journal.pntd.0006167.
81. Mutso M, Saul S, Rausalu K, Susova O, Zusinaite E, Mahalingam S, Merits A. 2017. Reverse genetic system, genetically stable reporter viruses and packaged subgenomic replicon based on a Brazilian Zika virus isolate. J Gen Virol 98:2712–2724. https://doi.org/10.1099/jgv.0.000938.